



Structural Geology of the Turtle Mountain Area near Frank, Alberta

Structural Geology of the Turtle Mountain Area near Frank, Alberta

C.W. Langenberg¹, D. Pană¹, B.C. Richards²,
D.A. Spratt³ and M.A. Lamb³

¹Alberta Energy and Utilities Board
Alberta Geological Survey

²Geological Survey of Canada

³University of Calgary

March 2007

©Her Majesty the Queen in Right of Alberta, 2007
ISBN 0-7785-3839-7

The Alberta Energy and Utilities Board/Alberta Geological Survey (EUB/AGS) and its employees and contractors make no warranty, guarantee or representation, express or implied, or assume any legal liability regarding the correctness, accuracy, completeness or reliability of this publication. Any digital data and software supplied with this publication are subject to the licence conditions. The data are supplied on the understanding that they are for the sole use of the licensee, and will not be redistributed in any form, in whole or in part, to third parties. Any references to proprietary software in the documentation and/or any use of proprietary data formats in this release do not constitute endorsement by the EUB/AGS of any manufacturer's product.

When using information from this publication in other publications or presentations, due acknowledgment should be given to the EUB/AGS. The following reference format is recommended:

Langenberg, C.W., Pană, D., Richards, B.C., Spratt, D.A. and Lamb, M.A. (2007): Structural geology of the Turtle Mountain area near Frank, Alberta; Alberta Energy and Utilities Board, EUB/AGS Earth Sciences Report 2007-03, 46 p.

Published March 2007 by:

Alberta Energy and Utilities Board
Alberta Geological Survey
4th Floor, Twin Atria Building
4999 – 98th Avenue
Edmonton, Alberta
T6B 2X3
Telephone: (780) 422-3767 (Information Sales)
Fax: (780) 422-1918
E-mail: EUB.AGS-Infosales@eub.ca
Website: www.ags.gov.ab.ca

Contents

Acknowledgments	v
Abstract	vi
1 Introduction	1
2 Methodology	1
2.1 Mapping	1
2.2 Image Logs	3
2.3 Palliser Formation.....	9
2.4 Banff Formation.....	9
2.5 Livingstone Formation.....	10
2.6 Mt. Head Formation.....	10
2.6.1 Salter/Baril/Wileman Members	10
2.6.2 Loomis Member	10
2.6.3 Carnarvon/Marston Members.....	10
2.7 Etherington Formation.....	10
2.8 Tobermory Formation.....	11
2.9 Fernie Formation.....	11
2.10 Kootenay Group.....	11
2.11 Blairmore Group.....	11
3 Structural Geology	12
3.1 Macroscopic Structures	12
3.1.1 Folds	12
3.1.2 Faults	14
3.1.3 Fissures.....	14
3.2 Mesoscopic Structures.....	14
3.2.1 Thrusts.....	14
3.2.2 Normal Faults	16
3.2.3 Strike-Slip Faults.....	16
3.2.4 Folds	16
3.2.5 Fractures (Joints)	16
4 Implications for Slope Stability	21
5 References	23
Appendix 1. Section 97RAH4 Blairmore A	25
Appendix 2. Section 97RAH5 Blairmore B	26
Appendix 3. Section 98RAH14 Blairmore C	27
Appendix 4. Open Fissures near South Peak	28
Appendix 5. Fractures Measured in Scan Line near Borehole	29
Appendix 6. Fractures Measured in Scan Line near Crack #1	30
Appendix 7. Fractures Measured in Scan Line near Crack #2	31
Appendix 8. All Subsurface Structural Data (from Borehole)	32

Tables

Table 1.	Fracture density and spacing in outcrop and borehole.....	20
----------	---	----

Figures

Figure 1	Map of Turtle Mountain area.....	13
Figure 2	Geological map of the Turtle Mountain area.....	14
Figure 3	Cross-sections through Turtle Mountain.....	15
Figure 4	Example of Turtle Mountain RGB and converted image logs and tadpole plot.....	16
Figure 5	Simplified stratigraphic column of the Turtle Mountain area.....	17
Figure 6	The correlation of the various Devonian and Carboniferous lithostratigraphic units of southwest Alberta and adjacent regions.....	18
Figure 7	The Turtle Mountain anticline outlined by carboniferous sediments along Drum Creek.....	19
Figure 8	Equal area stereoplot of poles to bedding orientation in the South Peak area.....	20
Figure 9.	Equal area stereoplot of poles to bedding orientation in an area south of South Peak.....	21
Figure 10	Aerial photo of South Peak with stereonet of fractures and fissures.....	22
Figure 11	Example of a wide open 'major fracture' (light blue) with other fractures (dark blue) imaged in a portion of the Turtle Mountain borehole.....	23
Figure 12	Equal area stereoplot of poles to normal faults.....	24
Figure 13	Equal area stereoplot of poles to strike slip faults.....	25
Figure 14	A mesoscopic fold in sandstone and shale overlying Seam #1.....	26
Figure 15	Equal area stereoplot of poles to fractures from the whole area.....	27
Figure 16	Stereonet of poles to all surface fractures in the South Peak area.....	28
Figure 17	Stereoplot of poles to all fractures and major fractures in the borehole.....	29
Figure 18	Borehole data superimposed on GPR data interpretation (thin lines) of Theune et al., 2006.....	30

Acknowledgments

Greg Carter, Dave Redman, Ron Wolsey (Emergency Management Alberta) and Monica Field (Alberta Community Development) are thanked for co-managing the Turtle Mountain Monitoring Project from 2003 until 2005. Staff at the Frank Slide Interpretive Centre is thanked for facilitating our field work. Corey Froese and John Waldron are thanked for reviewing this report. Rod Read and Dave Cruden are thanked for discussing geotechnical aspects of the project with us.

Abstract

Turtle Mountain forms part of the Livingstone Thrust sheet of the Foothills in southwest Alberta and consists of Paleozoic carbonates and Mesozoic clastics. The dominant geological structures on Turtle Mountain are the Turtle Mountain anticline and the Turtle Mountain Thrust. The rocks forming the mountain are Paleozoic strata of the Palliser, Banff, Livingstone, Mount Head, Etherington and Tobermory formations.

A detailed geological map of the South Peak area allows the construction of down-plunge cross-sections, displaying the various structures. The Turtle Mountain anticline changes geometry along its trend. Near the top of South Peak it forms a type of box fold with a 2° NNE plunging fold axis.

The Turtle Mountain anticline is a modified fault-propagation fold and can be described as a break-thrust fold. The rocks are extensively fractured. The Paleozoic carbonates are of most interest regarding the stability of the mountain. Fracture fabrics of these carbonates were measured in outcrop and obtained from image logs in a borehole. The majority of fractures are extension fractures with accompanying shear fractures related to the anticlinal fold.

Two main types of slope failure mechanisms can be distinguished: sliding and toppling. Sliding along bedding planes along the east limb of the Turtle Mountain anticline near South Peak could result in a major rock slide toward Bellevue. Normal faults are the main structures causing topple failure. They are slightly more likely to occur in the North Peak area and will generally be smaller in volume than the potential South Peak slide.

1 Introduction

The Province of Alberta committed to implementing a state-of-the-art monitoring system for Turtle Mountain on April 29th, 2003. This system might provide early warnings for future rock slides from the South Peak of Turtle Mountain. EUB/AGS cooperated with Emergency Management Alberta (Municipal Affairs) and Community Development in the implementation of the Turtle Mountain Monitoring System (Read et al., 2005). EUB/AGS was funded to perform a structural geological study and to provide a new geological map and cross-sections for the project. The results of this work are presented in this report.

The Alberta Geological Survey was involved with the stability of Turtle Mountain in the 1930s and issued some significant (unfortunately unpublished) reports (Allan, 1931, 1932, 1933). Cruden and Krahn (1973) provide a more recent geological model. Fossey (1986) provides a geological map and cross-sections of the South Peak area. The area also forms part of the area mapped at a 1:50,000 scale by Norris (1993). Richards et al. (2000) provide a regional framework for the Carboniferous stratigraphy.

The present report describes the structural geology of the Turtle Mountain area. It includes the subsurface fracture study by Spratt and Lamb (2005). The location of the Turtle Mountain area is shown in Figure 1.

2 Methodology

2.1 Mapping

The area was mapped by measuring stratigraphic sections (appendices 1-3), visiting outcrops, recording stratigraphic units and measuring structural elements such as bedding, faults and fractures, which were measured in outcrop with a structural compass. Outcrops were located on detailed aerial photographs with scales of 1:2000 to 1:20,000 and coordinates of outcrops were obtained by handheld GPS. Major joint planes were measured in many outcrops visited. In addition, fractures along three straight scan lines (LaPointe and Hudson, 1985) were measured. The straight scan line technique involves a traverse along a measuring tape, along which all visible fracture planes are measured and their positions are recorded so that fracture densities and spacing could be determined. SpheriStat 2.2TM was used for field data compilation and statistical analysis of structural data. The geology is summarized in Figure 2.

The orientations and positions of cross-sections were chosen based on possible slide paths of future rock slides. Cross-sections were aided by down-plunge projection of bedding orientations (Charlesworth et al., 1976). The cross-sections are shown in Figure 3.

Structural elements (such as bedding, faults and fractures) were measured in outcrop with a structural compass. Major joint planes were measured in many outcrops visited. In addition, fractures along three straight scan lines (LaPointe and Hudson, 1985) were measured. The straight scan line technique involves a traverse along a line, along which all visible fracture planes are measured. From these data estimates on fracture density and spacing were obtained. Measurements on the orientation of open fissures are presented in Appendix 4 and the measurements of fractures along scan lines are presented in Appendices 5, 6 and 7.

A borehole was drilled for the microseismic program near the top of Turtle Mountain in order to place geophones in the subsurface (Bidwell et al., 2005). Structural elements along the walls of the borehole can be measured with the help of image logs (Spratt and Lamb, 2005). The ground surface was set as the datum for drilling and logging, and the borehole was drilled to a depth of 61.3 m (fluid = air). Surface

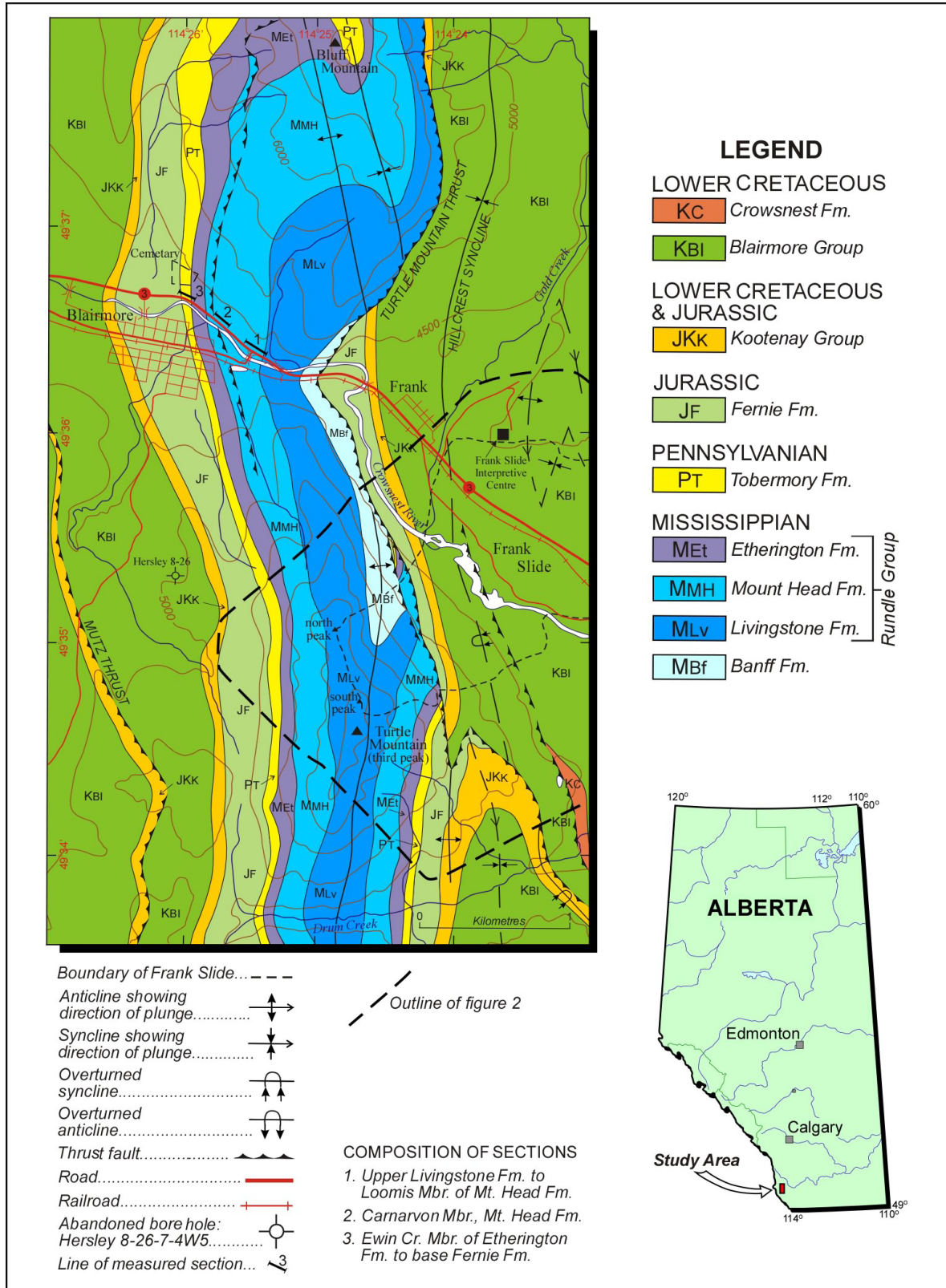


Figure 1. Map of Turtle Mountain area. The geology is from Norris, 1993. The outline of the map of Figure 2 is given. The measured sections are presented in Appendices 1 to 3.

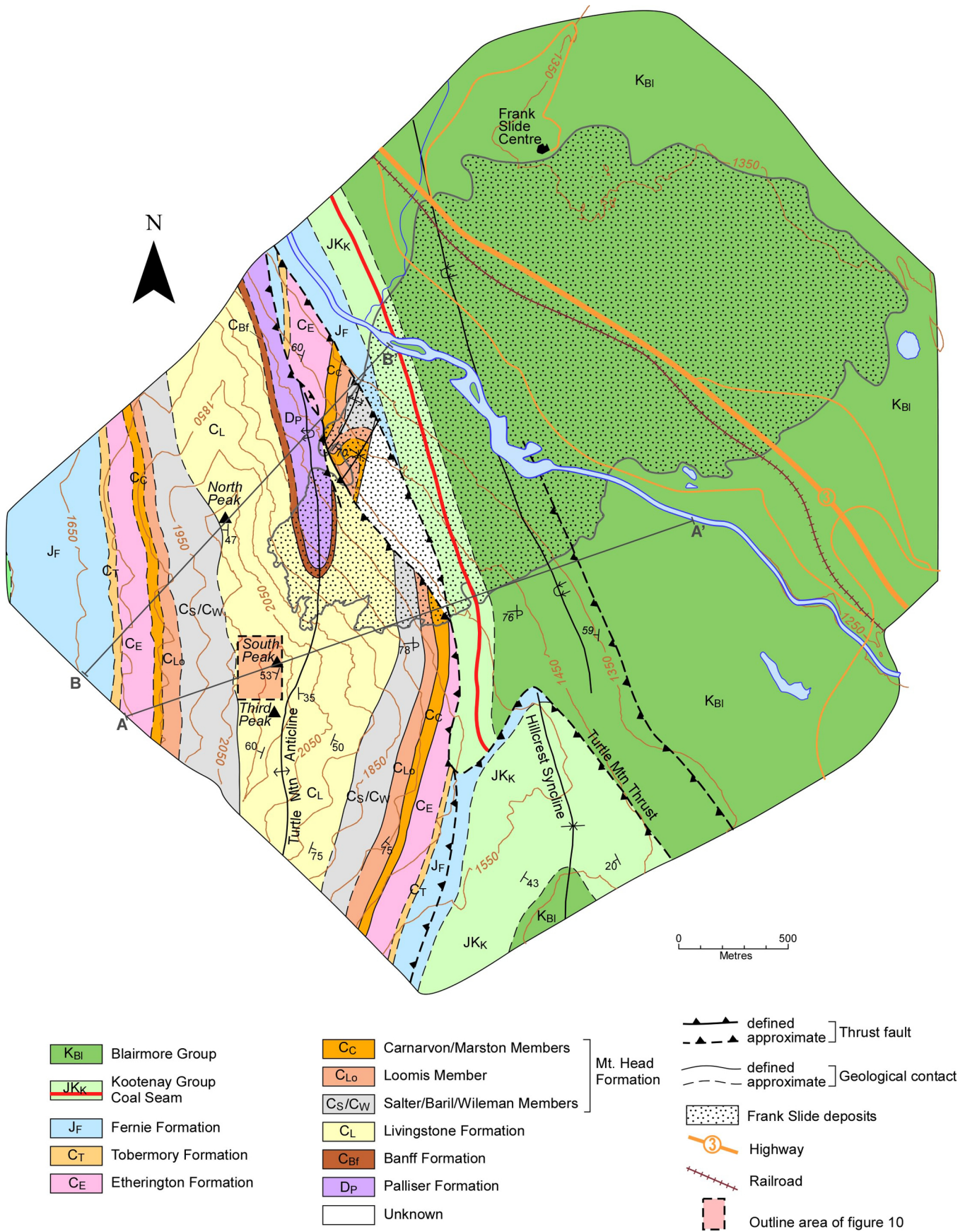


Figure 2. Geological map of the Turtle Mountain area.

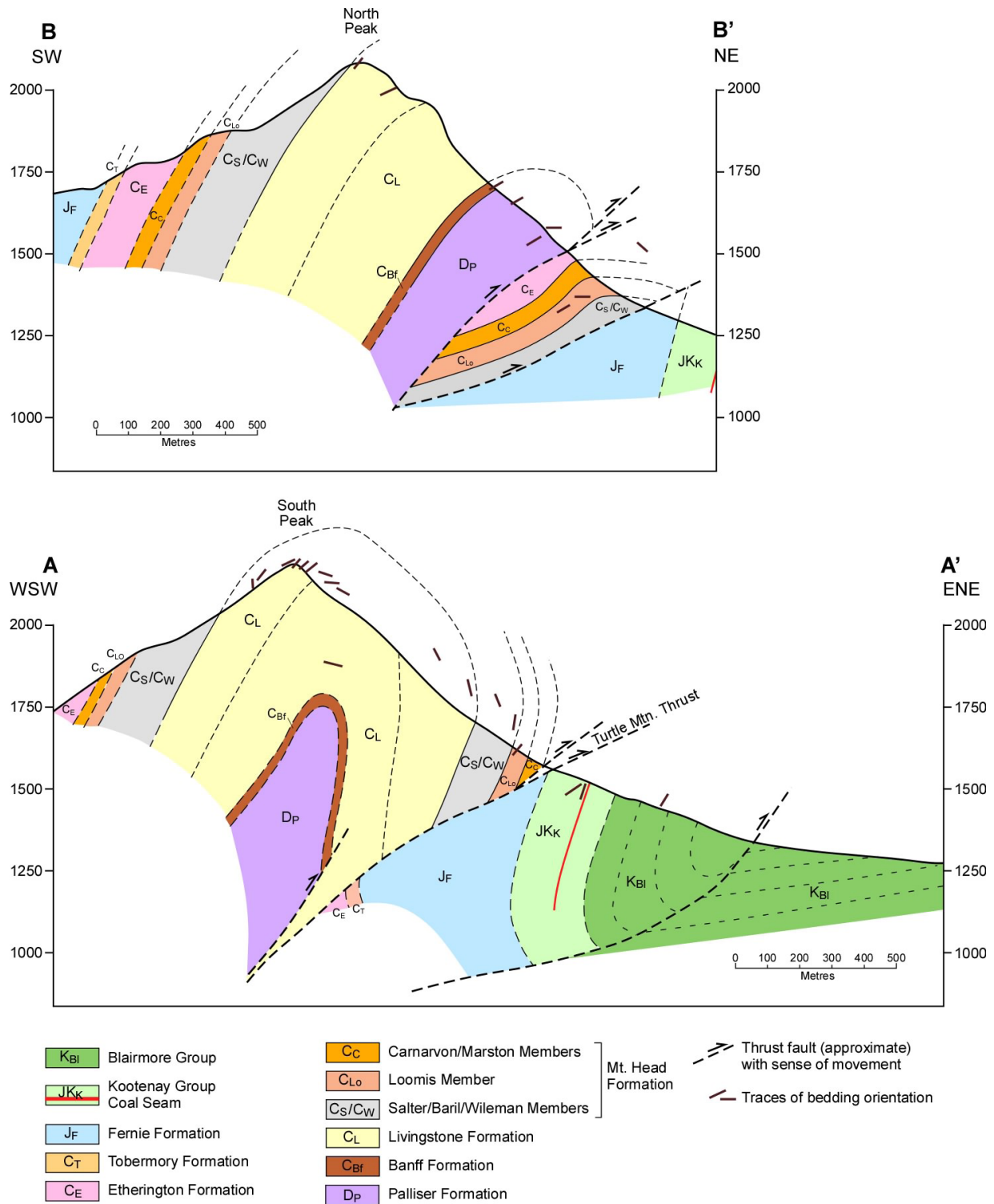


Figure 3. Cross-sections through Turtle Mountain. The cross-section lines are indicated on Figure 2.

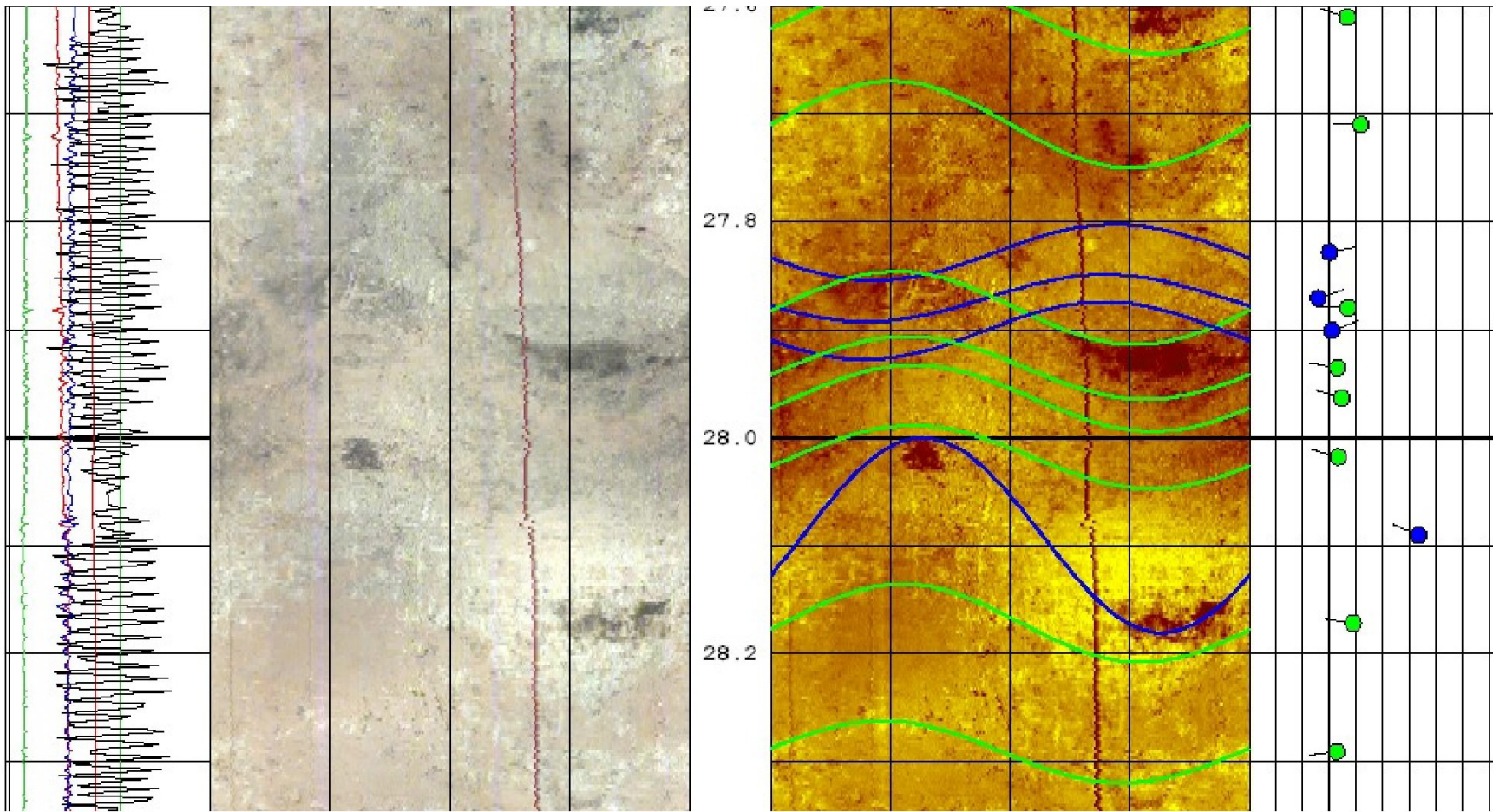


Figure 4. Example of Turtle Mountain RGB and converted image logs and tadpole plot. Green sinusoids parallel bedding; blue sinusoids parallel fractures. See text for details.

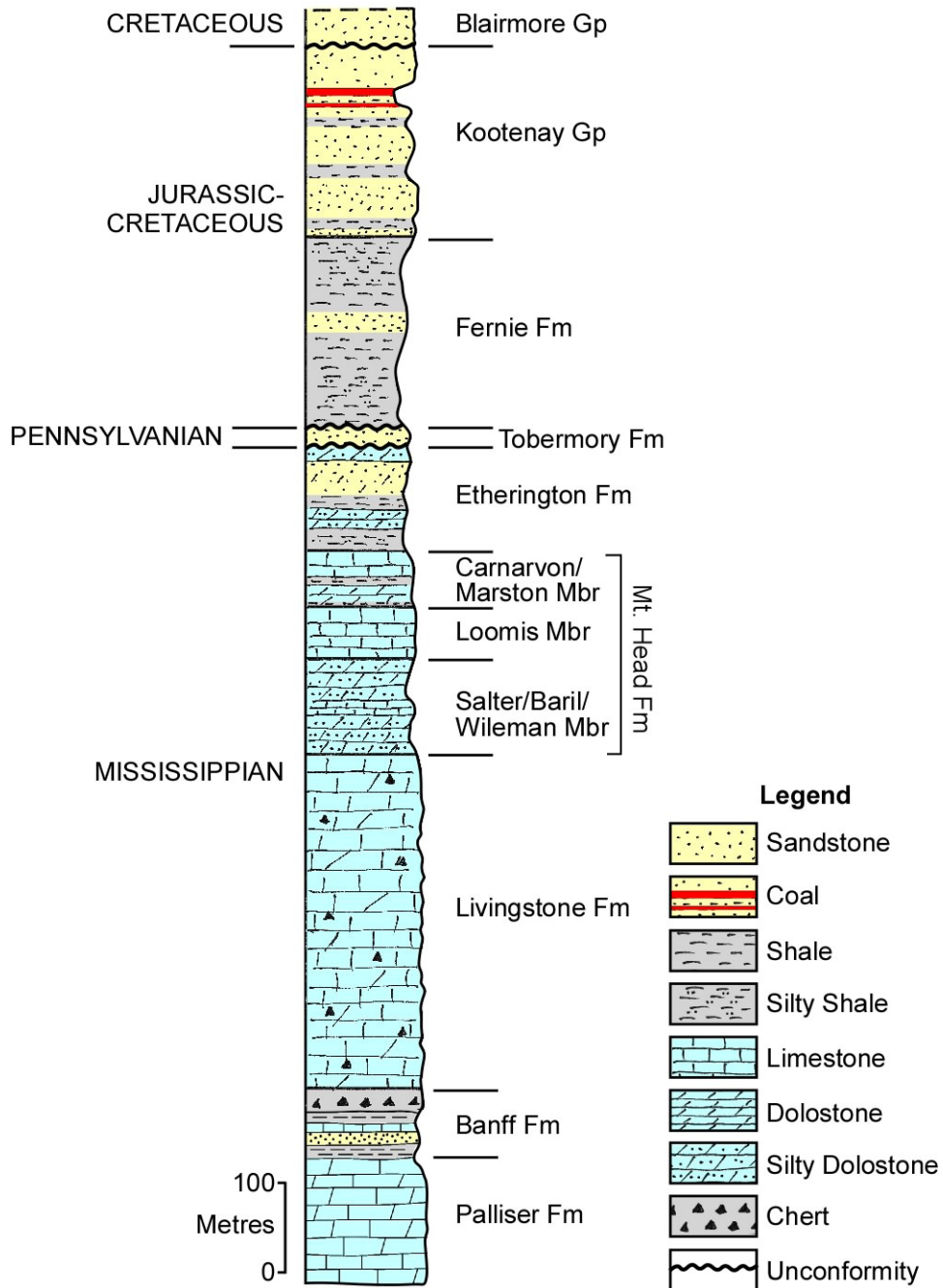


Figure 5. Simplified stratigraphic column of the Turtle Mountain area.

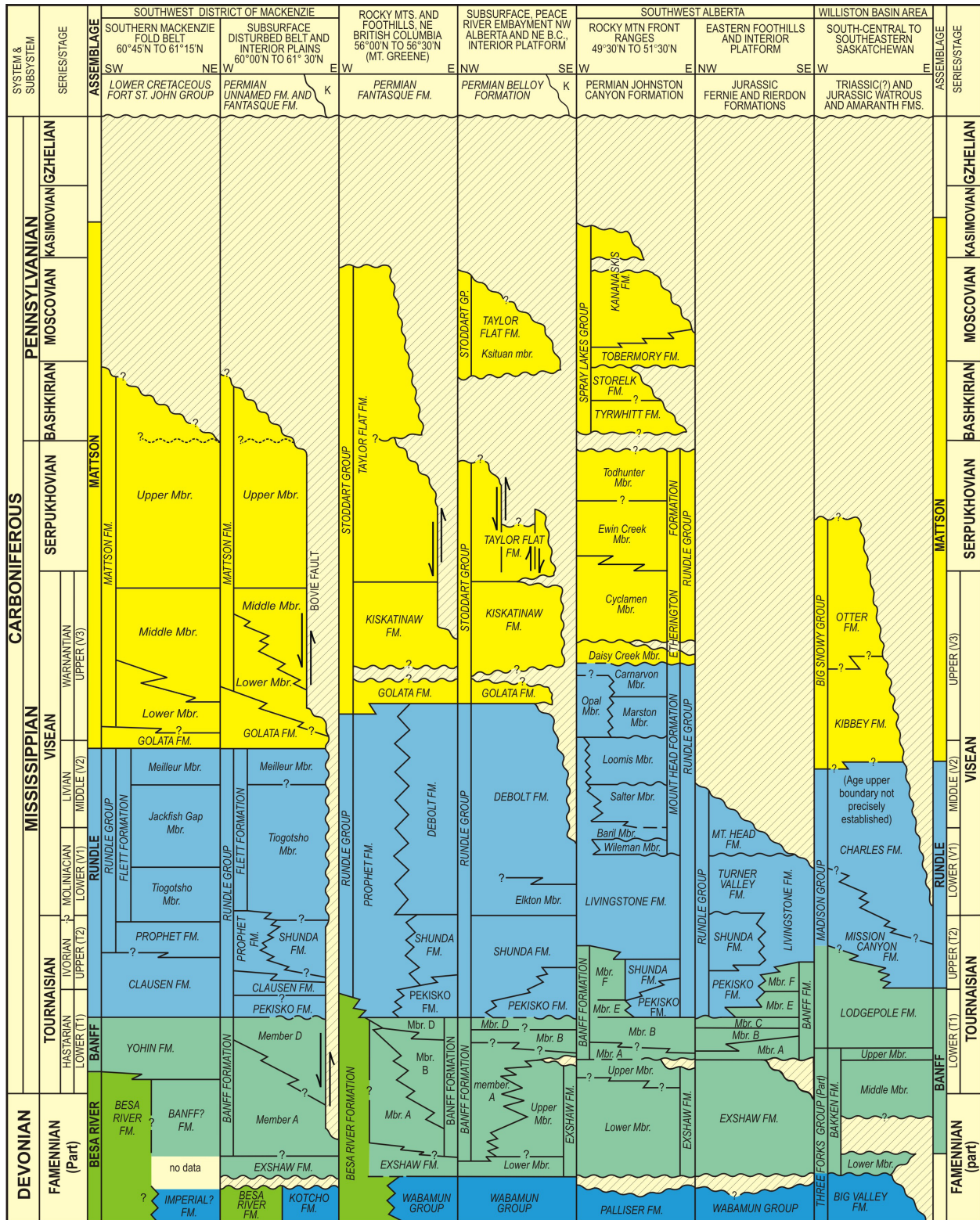


Figure 6. The correlation of the various Devonian and Carboniferous lithostratigraphic units of southwest Alberta and adjacent regions.



Figure 7. The Turtle Mountain anticline outlined by Carboniferous sediments along Drum Creek (view toward the south).

casing was set in the top 19.2 m of the borehole; the magnetometer was affected by the casing to a depth of 20.8 m; beyond this depth the next 40.5 m was reliably covered by image logs.

2.2 Image Logs

An Advanced Logic Technology (ALT) Obi40 digital optical televiewer was used to image the wall of the Turtle Mountain borehole, as acoustic logging tools cannot operate in air-filled boreholes. The ALT Obi40 tool consists of a directional device and an imaging device. The directional device is made up of two accelerometers to determine the deviation of the tool from vertical and a precision three-axis magnetometer to orient the image relative to magnetic north. The imaging device consists of a downhole charged-couple device (CCD) camera directed onto a rotating prism and multi light-emitting diode (LED) source. As the prism rotates, the CCD is directed at a different section of the borehole. Depending on the frequency of the image gathered from the CCD, up to one image per degree of rotation can be obtained. High-output LEDs are placed in a ring around the tool adjacent to the prism to illuminate the borehole and to provide a light source for the CCD image capture. These images are acquired continuously as the tool is moved up the borehole, providing a 360° continuous image of the surface of the wellbore.

The Turtle Mountain borehole image logs are presented using WellCad™ software (Figure 4). The direct RGB images are shown in the second track (grey image). The RGB image is then converted into a histogram image on which features such as bedding and fracture planes can be identified. The converted image is the reddish brown image on the right. Sinusoids on the converted image represent planar surfaces and are interpreted as bed boundaries (green), fractures (blue) and major open fractures (light blue), which have apertures >1 cm. Due to the nature of the rock (relatively homogeneous carbonate) the bedding is difficult to pick out, but it is best seen on the RGB image where gradational light-dark bands, some with vugs, are present and have sinusoidal contacts. Open cracks and planar features that are not

parallel to bedding are interpreted to be fractures. Each feature that looks as if it could be bedding or a fracture plane is visually picked and then tested for planarity using WellCad's sinusoid-fitting tool. If a feature is not planar, it will not fit a sinusoid and it is therefore not recorded for structural analysis. The amplitude of the sinusoid and the position of its trough define the dip and dip direction of the plane that fits the sine curve. The recorded depth of the feature in the borehole is taken as the depth of the inflection points (midpoints) of the sinusoid. These data are displayed as tadpoles in the right hand track of the log. The position of the dot identifies the depth in the well and true dip (0° on the left, 90° on the right) of the plane, and the tail of the tadpole points in the true dip direction (with magnetic north being at the top of the page and south at the bottom). The first track includes directional information including the azimuth of the borehole (Azimuth), deviation of the borehole from vertical (Tilt) and various other tool readings used to orient the tool. The Turtle Mountain borehole has an average trend of 049° and average deviation of 6° from vertical (plunge = 84°).

The quality of the image logs is excellent, much better than anticipated considering the number of large cracks near the borehole site. Surface casing was set in the top 19.2 m of the borehole, and the magnetometer was affected by the casing to a depth of 20.8 m, but reliably oriented and continuous logs were collected to the bottom of the hole. The entire 40.5 m of the image log was interpreted. The orientation of structural elements observed along the borehole is presented in Appendix 8.

Bedding was consistently oriented over the logged interval, with a mean dip and dip direction of $37^\circ/294^\circ$ (strike and dip: $204^\circ, 37^\circ\text{W}$).

Stratigraphy

Rocks in the area range in age from Devonian to Cretaceous. A simplified stratigraphic column is presented in Figure 5. A good section of the Carboniferous rocks of the area is located along Highway 3 near Blairmore, which includes strata from the Banff Formation to the Tobermory Formation. This section consists of three parts with two covered intervals in between and may contain a thrust fault (Figure 1). Part 1 includes the section from Upper Livingstone Formation to Loomis Member of the Mt. Head Formation (Appendix 1), Part 2 is largely the Carnarvon Member of the Mt. Head Formation (Appendix 2), and Part 3 includes a section from the Ewin Creek Member of the Etherington Formation to base of Fernie Formation (Appendix 3). This section defines a reference section for the Mount Head, Etherington and Tobermory formations. The correlation of the various Devonian and Carboniferous lithostratigraphic units of southwest Alberta and adjacent regions is shown in Figure 6.

2.3 Palliser Formation

The Devonian (Famennian) Palliser Formation is represented by fractured burrow-mottled dolomitic limestone and is about 150 m thick. It most likely represents the Morro Member. It is located in an area referred to as the 'Hoodooos.' These types of hoodoos are formed because of the close to vertical orientation of the bedding planes in this area (Figure 2). The Exshaw Formation may be part of this interval, but it could not be determined with certainty because the top of this section is covered. The Palliser Formation rocks form a minor component of the Frank Slide deposits.

2.4 Banff Formation

The Tournaisian (Mississippian) Banff Formation is represented by about 50 m of section, consisting of black mudstone, siltstone, sandstone, banded chert, and dark grey to black, cherty, sometimes argillaceous limestone. A prominent band of about 10 m thick banded chert is located near the top of the formation, forms a marker horizon and can be mapped on the east slope of Turtle Mountain from the edge of the 1903 Frank Slide northward to the gap of the Crowsnest River. The Banff Formation rocks form a minor component of the Frank Slide deposits.

2.5 Livingstone Formation

The Tournaisian to Visean (Mississippian) Livingstone Formation consists mainly of massive, grey, fine to coarse-crystalline limestone (predominantly pelmatozoan lime grainstone). In addition, cherty, grey limestone and dolostone occurs. The rocks of the Livingstone Formation of southwestern Alberta include strata equivalent to the Shunda and Turner Valley formations of Central Alberta (Richards et al., 2000). The Livingstone Formation forms the crest of Turtle Mountain and is the main rock of the 1903 Frank Slide deposits. From cross-section AA' (Figure 3) the thickness of the Livingstone Formation at Turtle Mountain can be estimated at 350 m.

2.6 Mt. Head Formation

The Visean (Mississippian) Mt. Head Formation includes the Wileman, Baril, Salter, Loomis, Marston and Carnarvon members (Richards et al., 2000). The Baril and Marston members could not be mapped consistently on Turtle Mountain and consequently the Mt. Head was divided into three mappable units: 1) Salter/Baril/Wileman members, 2) Loomis Member and 3) Carnarvon/Marston members. The total thickness can be estimated from the cross-sections at 220 m. The Mt. Head Formation rocks form a minor component of the Frank Slide deposits.

2.6.1 Salter/Baril/Wileman Members

The generally recessive Salter/Baril/Wileman members are dominated by dolomitic siltstone grading into finely crystalline silty dolostone. These are the lithologies of the Wileman and Salter members. They commonly contain white carbonate nodules and sedimentary breccias. Plant remains may be present. In addition, some (peloid skeletal) lime grainstone units occur which are similar to the Baril Member. However, these units do not occur in a consistent stratigraphic position (some are in the lower part and some in the middle part of the map unit) and for that reason the Baril Member could not be separated on the map. This unit is about 65 m thick along the Highway near Blairmore and may be up to 100 m thick in the study area according to the mapping of Turtle Mountain.

2.6.2 Loomis Member

Cliff forming carbonates of the Loomis Member consist of grey lime grainstone. This unit is about 60 m thick.

2.6.3 Carnarvon/Marston Members

Resistant, well-bedded carbonates comprise the Carnarvon/Marston members and form an easily mappable unit. Recessive beds of mudstone are rhythmically interlayered with the resistant carbonate beds. This gives the Carnarvon its characteristic well-bedded aspect. The Marston Member is the lowest of these interbedded mudstone units, but it is nowhere clearly exposed. Consequently, the unit could not be mapped as a separate member and is included in the Carnarvon/Marston map unit. This unit is about 60 m thick. In the southern part of the map area (near Drum Creek), the unit mapped as Carnarvon/Marston members shows a transition to the Opal Member with a more open marine character (Richards et al., 1994).

2.7 Etherington Formation

The Visean to Serpukhovian (Mississippian) Etherington Formation includes the Daisy Creek, Cyclamen, Ewin Creek and Todhunter members (Richards et al., 2000). The Cyclamen, Ewin Creek and Todhunter members can be recognized along the highway section (Richards, in preparation), but they could not be mapped as separate units on Turtle Mountain. The Etherington Formation is generally recessive and

poorly exposed on Turtle Mountain and consists of (often dolomitic) carbonates grading into siliciclastic mudstone/siltstone. In addition, fine-grained (dolomitic) sandstone is present, especially near the top of the formation. The mudstones are often pale-greenish grey, but maroon mudstone is also present. The (dolomitic) sandstone often has a mottled appearance and, most likely, represents the Todhunter member. The Todhunter Member is unconformably overlain by the Pennsylvanian Tobermory Formation. The Etherington Formation is about 110 m thick.

2.8 Tobermory Formation

The sandstone dominated Pennsylvanian (Bashkirian to Moscovian?) Tobermory Formation (Scott, 1964) was mapped as the Misty Formation by Norris (1993). Major unconformities exist at the top (Pennsylvanian/Jurassic unconformity) and the base (Mississippian/Pennsylvanian unconformity) of this formation. Most of the Tobermory comprises fine-grained, silty sandstone grading into sandy siltstone, but beds of silty dolostone and argillaceous siltstone grading into mudstone occur. Along Highway 3 near Blairmore, the lower 40 cm of the formation is a bed of granule to pebble conglomerate and breccia. The Tobermory Formation can be estimated to be about 20 m thick (it is 17 m along the Highway near Blairmore).

2.9 Fernie Formation

The Fernie formation is not completely exposed in the Turtle Mountain area but the lower part of the unit is exposed on the north side of Highway 3 in Blairmore and fine-grained sandstone representing the passage beds are exposed at one outcrop along the Crownsnest River. A reliable thickness could not be determined.

2.10 Kootenay Group

The Jurassic/Cretaceous Kootenay Group (Gibson, 1985) consists of the Morrissey Formation at the base and the coal-bearing Mist Mountain Formation at the top. However, they could not be mapped as separate units and are shown as one unit (Kootenay Group). The Kootenay Group consists of fine to coarse-grained grey sandstone and siltstone, dark grey and black carbonaceous mudstone and coal. The most prominent coal seam (Seam #1, see MacKay, 1933) is 3 to 6 m thick and was mined in the Frank Coal Mine. Another coal seam (Seam #2) is situated about 12 m below Seam #1 and is about 2 m thick. The top of the Kootenay Group is not well defined. MacKay (1933) placed the top of the Group immediately above Coal Seam #1 at the base of prominent fine-grained sandstones exposed along the Crownsnest River and in the coal collapse pits on the east slope of Turtle Mountain. It is uncertain if these sandstones are the Dalhousie sandstones (Leckie and Cheel, 1997). It seems more likely that these sandstones belong to the Kootenay Group of the Blairmore Group, and consequently, the unconformable contact between Kootenay and Blairmore Group was tentatively placed above these sandstones (see Figure 2). The thickness of the Kootenay Group is estimated to be about 200 m.

2.11 Blairmore Group

The Cretaceous Blairmore Group consists of the Cadomin/Dalhousie, Gladstone, Beaver Mines and Mill Creek formations (Leckie and Cheel, 1997). No attempts were made to map any of these units and the Blairmore Group is shown as one undifferentiated unit. The group comprises sandstone, siltstone and mudstone. Some good exposures of igneous-clast conglomerate (Leckie and Krystinik, 1995) are present close to the Frank Slide Interpretive Centre. A major unconformity is present at the base of the Blairmore Group, but this contact is difficult to map (see above).

3 Structural Geology

The visible structures on Turtle Mountain can be divided into macroscopic and mesoscopic structures.

3.1 Macroscopic Structures

The large-scale structures can be divided into folds, faults and fissures.

3.1.1 Folds

The Turtle Mountain anticline is the most prominent structure in the area and is outlined by the Carboniferous sediments (Figure 7). Near South Peak it forms a type of box fold (see Figure 3). The fold axis in the South Peak area plunges 2° toward azimuth 024° (Figure 8). An analysis of the distribution of the poles to bedding in this area indicates that a small circle with a half-apical angle of 83° can be fitted to the pole data, implying that the fold is slightly conical with a half-apical angle of 7° . The Turtle Mountain anticline is a modified fault-propagation fold and can be described as a break-thrust fold. The geometry of the fold changes along its trend as shown by varying inter-limb angles (see cross-sections of Figure 3). It also forms a hanging-wall anticline above the Turtle Mountain Thrust.

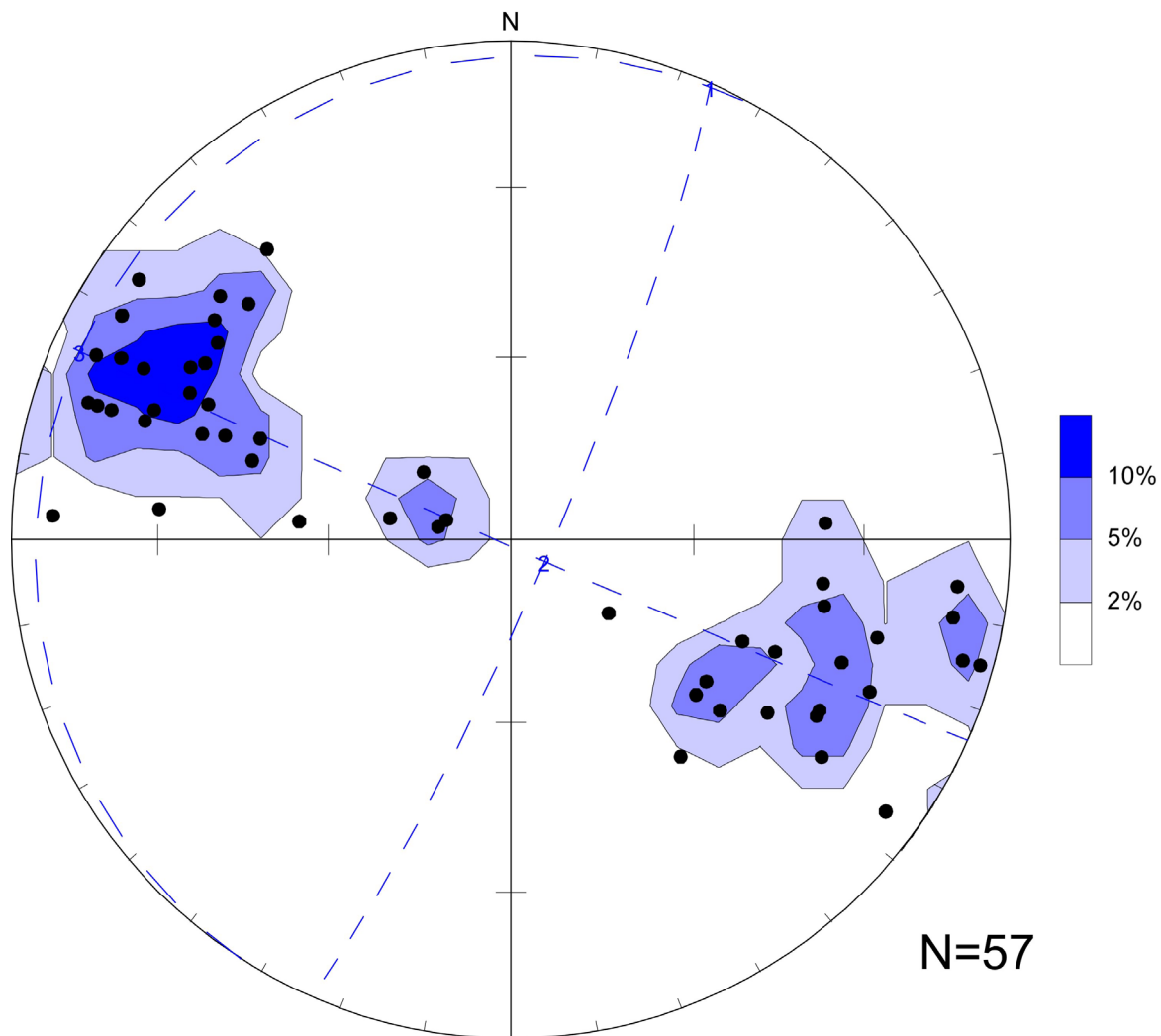


Figure 8. Equal area stereoplots of poles to bedding orientation in the South Peak area, defining the fold axis orientation. Contours at 2%, 5% and 10% of data per 1% of net.

The drillhole near South Peak intersected the west limb of the Turtle Mountain anticline where a mean dip and dip direction of $37^{\circ}/294^{\circ}$ of the bedding was determined from the image log data.

Further south, the fold axis of the Turtle Mountain anticline plunges 11° toward 201° (Figure 9). Folding appears to be cylindrical. The Hillcrest Syncline is the footwall syncline and is defined by Mesozoic strata. The fold axis trend is significantly different from the Turtle Mountain anticline; it trends west of north. This trend conforms to trends south of the Crowsnest Deflection, whereas the trend of the Turtle Mountain anticline conforms to trends north of this deflection (see map by Price, 1962). Both folds are displaced by the Turtle Mountain Thrust. However, the Turtle Mountain Thrust is also folded by the Hillcrest Syncline, indicating that folding took place both before and after the thrusting. Additional macroscopic folds (an anticline-syncline pair) are present in a thrust slice above the main Turtle Mountain Thrust. Their fold axes (plunging 7° toward 034°) are rotated clockwise from the orientation in the hanging wall around North Peak (plunging 1° toward 005°), most likely resulting from movements along the Turtle Mountain Thrust.

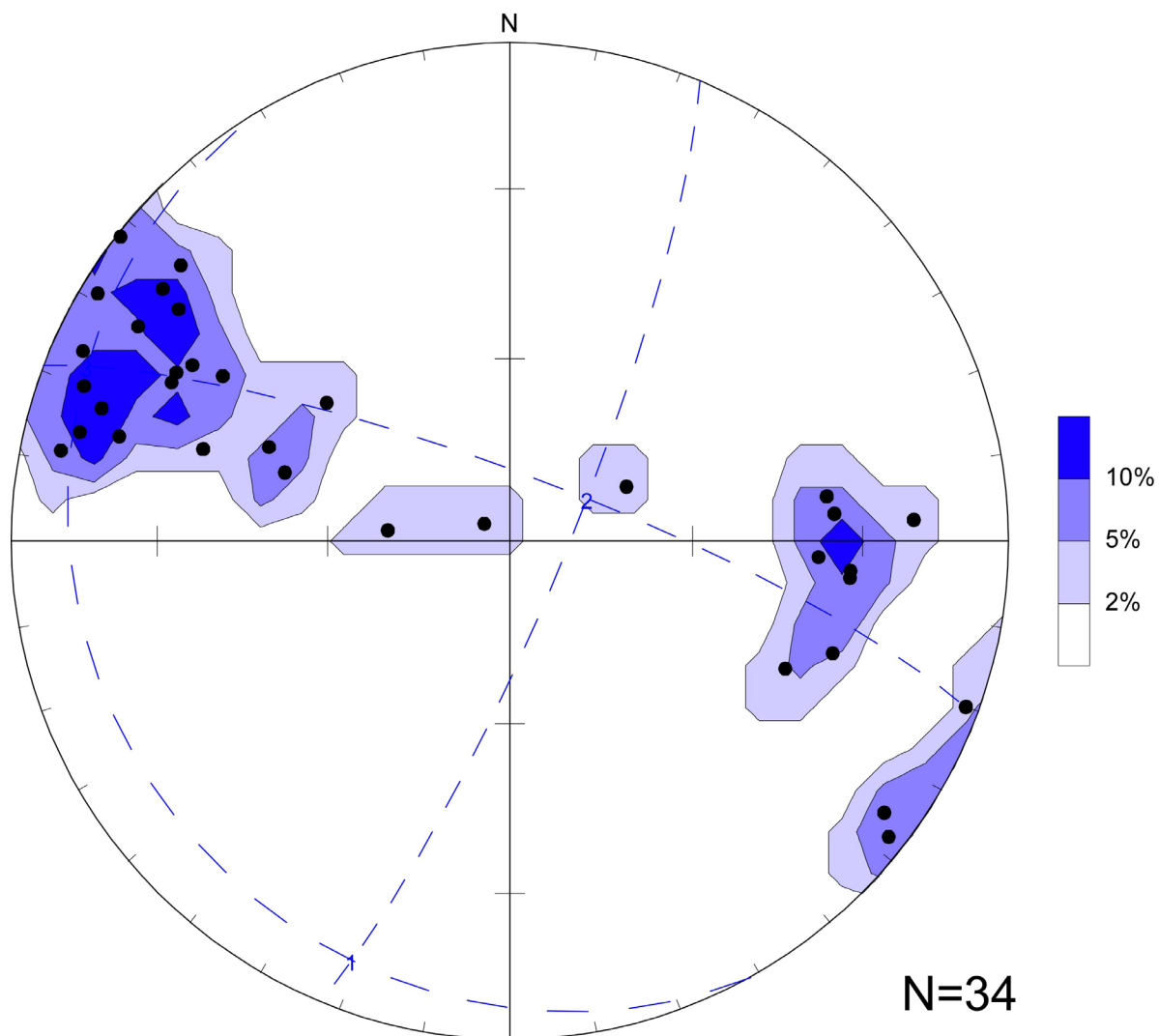


Figure 9. Equal area stereonet plot of poles to bedding orientation in an area south of South Peak, defining the fold axis orientation. Contours at 2%, 5% and 10% of data per 1% of net.

3.1.2 Faults

The Turtle Mountain Thrust is the main fault in the area. The fault is mainly located in the Fernie Formation, but cuts up-section to the Kootenay Formation. It seems likely that part of the displacement along this fault continues in the Fernie Formation to the South (Norris, 1993, shows a detachment in the Fernie Formation 5 km to the south). Part of the Turtle Mountain Thrust appears to be folded by the Hillcrest Syncline. The Turtle Mountain Fault contains a horse (thrust slice) in its hanging wall. Another (unnamed) thrust is present in the east limb of the Hillcrest Syncline.

The timing of movements along these faults is unknown. Movements probably started in the Paleocene and might still continue today, as indicated by small local seismic events along the fault observed by the Turtle Mountain microseismic system (Chen et al., 2005; Read et al., 2005). The main movements might have been around 52 Ma in the early Eocene (van der Pluijm et al., 2006).

3.1.3 Fissures

Major fissures (large open fractures) are present on the crest of Turtle Mountain. The main ones are identified as Crack #1 and #2 (Figure 10). Additional fissures are visible on this aerial photograph. The stereonet of 29 measurements of the orientation of these fissures (including various segments of Cracks #1 and #2) are shown in Figure 10 (“big open cracks”). The steep east-northeast dipping fissures can possibly form the back side of a potential future rock slide from South Peak. The widening of these fissures can be considered a neotectonic faulting process.

Several large open fractures, which can be considered fissures, were encountered in the borehole. Each has an aperture (width of opening perpendicular to the fracture surface) of more than 1 cm, as seen in the 1:5 scale image logs (Figure 11). Theoretical and field studies indicate that large aperture fractures are typically much longer than small aperture fractures, with 1 mm wide natural fractures being on the order of 1 m long and 1 cm wide fractures being on the order of 100 m long (e.g., Vermilye and Scholz, 1995). So the major fractures (> 1 cm aperture) in the borehole are the ones most likely to connect to fractures observed at the surface. Their orientations are shown in Figure 10 (open cracks in borehole). The most frequent dip directions of the large open fractures are to the northeast and east (toward the Frank Slide surface and the Town of Bellevue), and most of the dips are steeper than 60°. One major fracture dips west-northwest, subparallel to bedding; another dips south along the ridge. There is good correspondence with the orientation of the fissures (big open cracks) at the surface.

This indicates that the 40.5 m long image logs are representative of a wider area and that one can extrapolate information from the borehole. Geological maps based on surface mapping and air photographs tend to emphasize the steeply dipping fractures, whereas the subvertical borehole is able to detect potentially dangerous planes of weakness that were not obvious during field mapping. Together these datasets provide a complete sample of all the types of discontinuities that could contribute to slope instability.

3.2 Mesoscopic Structures

Mesoscopic structures present are thrusts, normal faults, strike-slip faults, folds and fractures. The faults were classified based on sense of movement.

3.2.1 Thrusts

Mesoscopic thrusts were observed in the area of the thrust slice and are indicated by the off-set of bedding planes and slickensides.

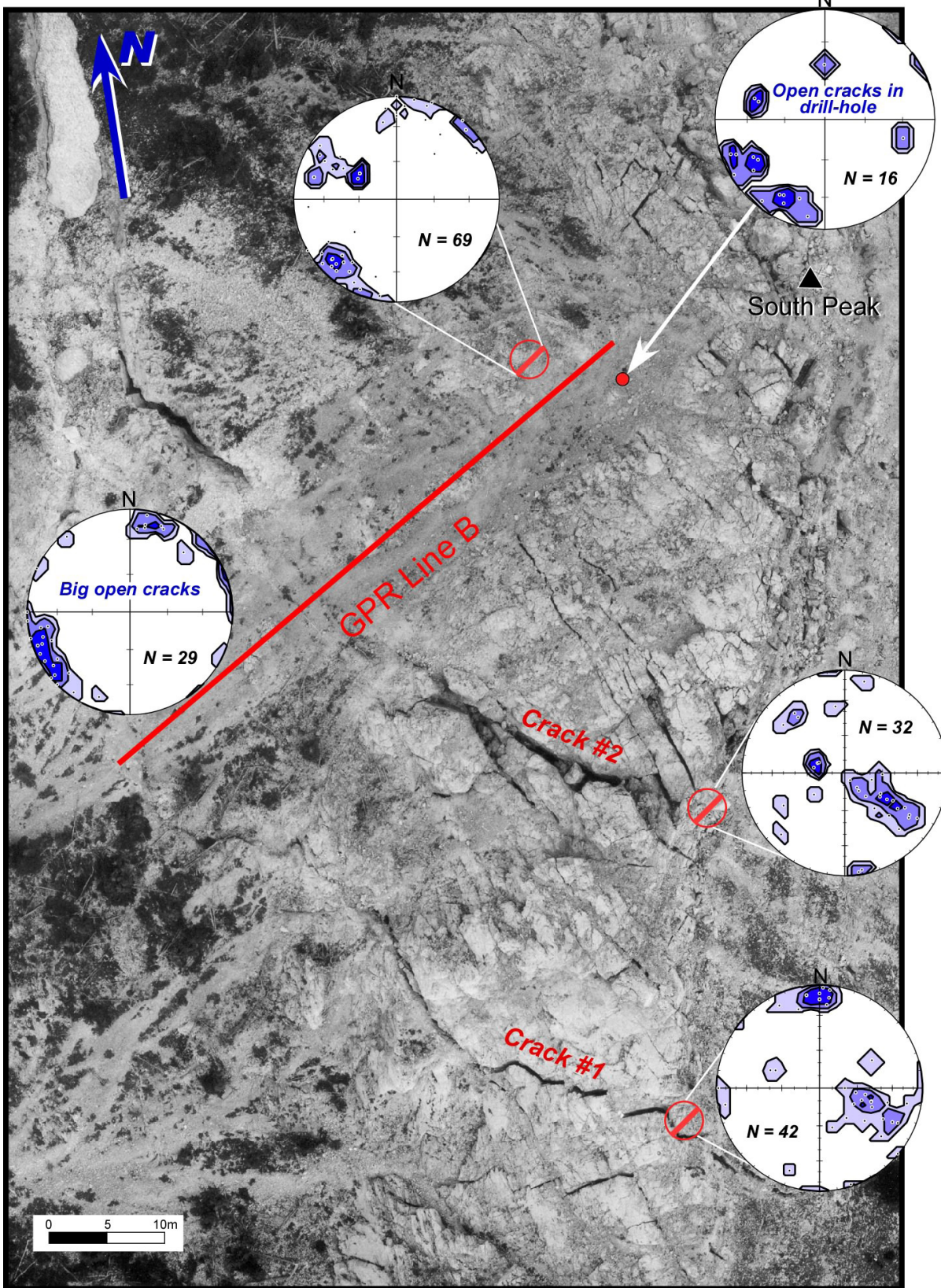


Figure 10. Aerial photo of South Peak with stereonets of fractures and fissures. The three scan lines are indicated by the red circles. The drillhole is shown with a red dot. The location of a GPR line (Figure 18) is also shown. See Figure 2 for location

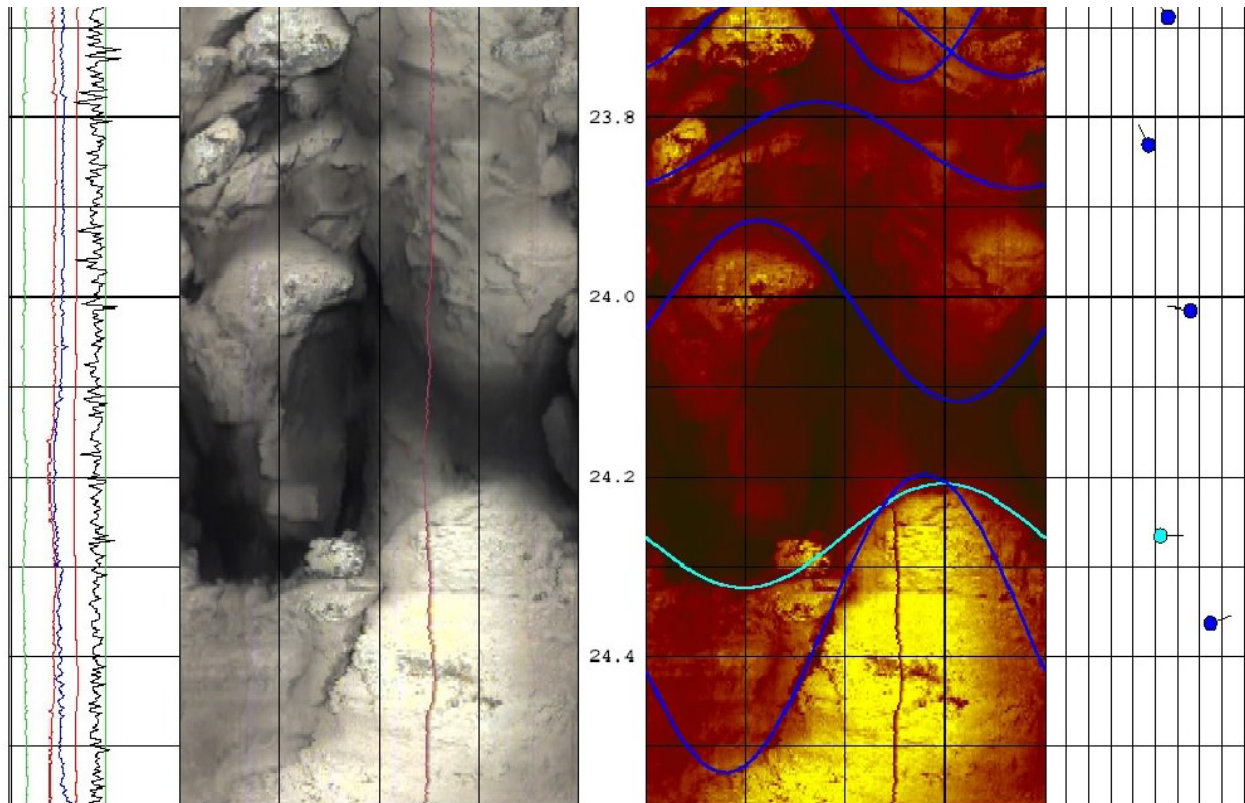


Figure 11. Example of a wide open 'major fracture' (light blue) with other fractures (dark blue) imaged in a portion of the Turtle Mountain borehole. See text for details.

3.2.2 Normal Faults

Normal faults are preferentially present in the Banff and Kootenay formations on the east slope of Turtle Mountain. Six orientations are given in Figure 12. Most of these normal faults appear to be neotectonic faults related to exfoliation of the east slope. A rock fall of 15 000 tonnes in June 2001 was initiated by such an exfoliation from the slope about 50 m below North Peak.

3.2.3 Strike-Slip Faults

Some of the steep faults show strike-slip movements as indicated by slickensides. Six measurements of the orientation of these strike-slip planes are shown in Figure 13.

3.2.4 Folds

A few mesoscopic folds were observed in the collapsed coal pits as shown in Figure 14.

3.2.5 Fractures (Joints)

Fractures (joints) are present in all exposures. The majority of fractures are extension fractures with accompanying shear fractures, which are related to the anticlinal fold. A sample of 66 measurements of prominent fractures from all outcrops visited is presented in Figure 15, but may be biased by outcrop location and orientation. A somewhat more representative sample is provided in measurements along three scan lines on the crest of Turtle Mountain (Figure 10). Joints along the scan line near the borehole have three dominant orientations, dipping moderately to steeply southeast, steeply northeast and steeply southwest. Less common fractures dip to the east-southeast, south-southeast and south-southwest (Figure

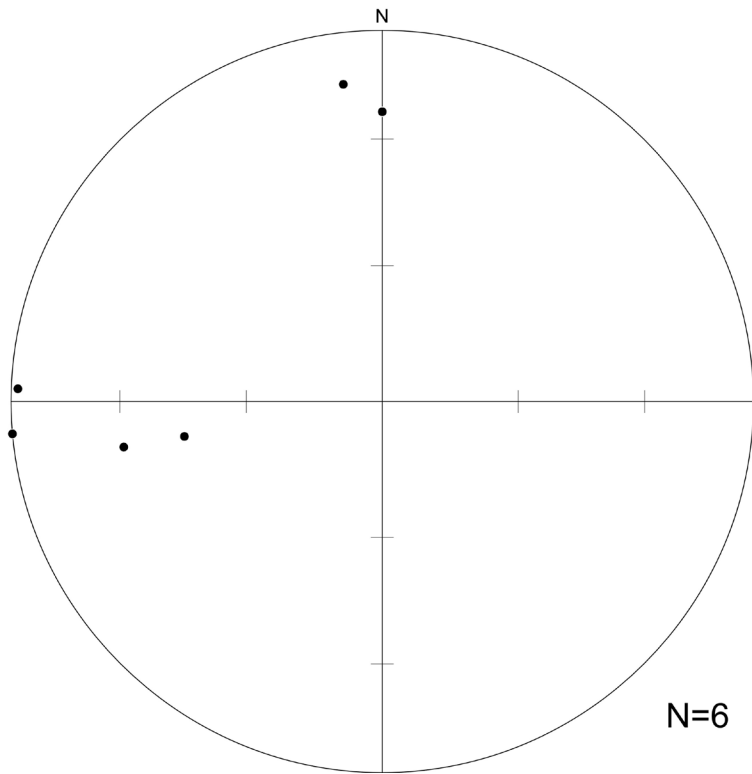


Figure 12. Equal area stereonet plot of poles to normal faults.

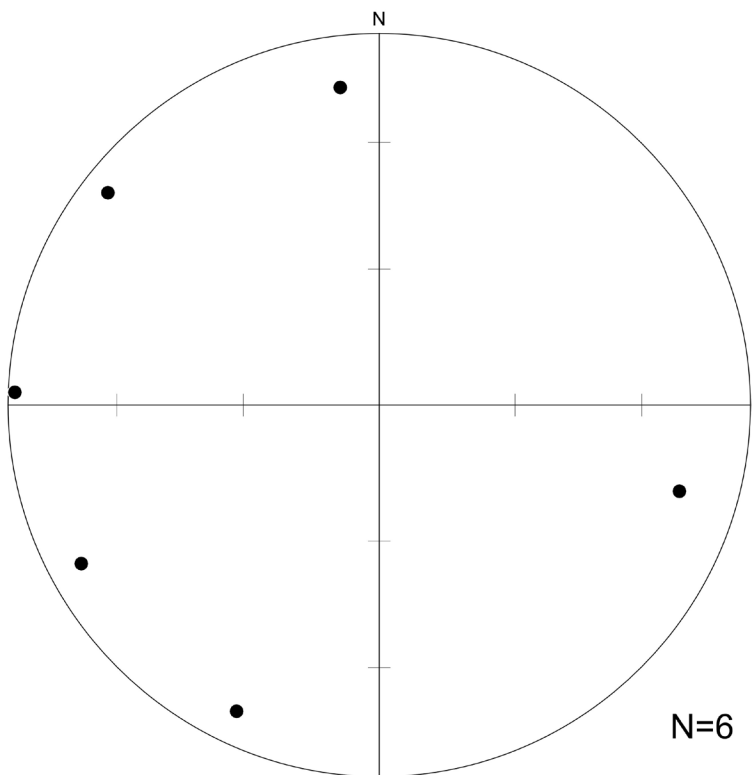


Figure 13. Equal area stereonet plot of poles to strike slip faults.



Figure 14. A mesoscopic fold in sandstone and shale overlying Seam #1.

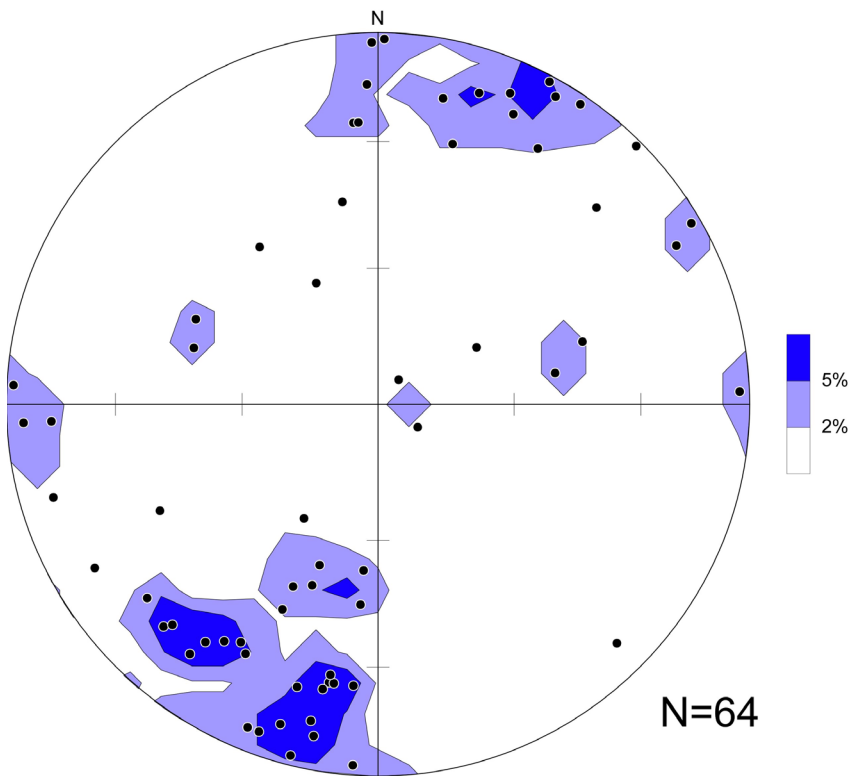


Figure 15. Equal area stereoplots of poles to fractures from the whole area. Contours at 2% and 5% of data per 1% of net.

10). The steeply northeast-dipping set (observed in the borehole and in the scan line near the borehole) will form the back side of a potential future rock slide from South Peak.

The two scan lines near Crack #1 and #2 show dominant fractures dipping 37° northwest, parallel to bedding, but there is another set of northwest-dipping fractures that is distinct and 15 to 20 degrees steeper, yielding the two modes of poles in the SE quadrant of the Crack #1 scan line. Also frequent are steeply south-dipping and shallowly south-southeast-dipping sets. Less common fractures dip shallowly to the southeast and moderately to the southwest.

All the data from the scan lines together with the data from the fissures are combined in Figure 16 to show all surface data on South Peak near the borehole. The three most frequent orientations seen are the northwest-dipping steeper-than-bedding set, the set dipping steeply northeast toward the Frank Slide surface and the set that dips $\sim 30^\circ$ southeast toward Hillcrest.

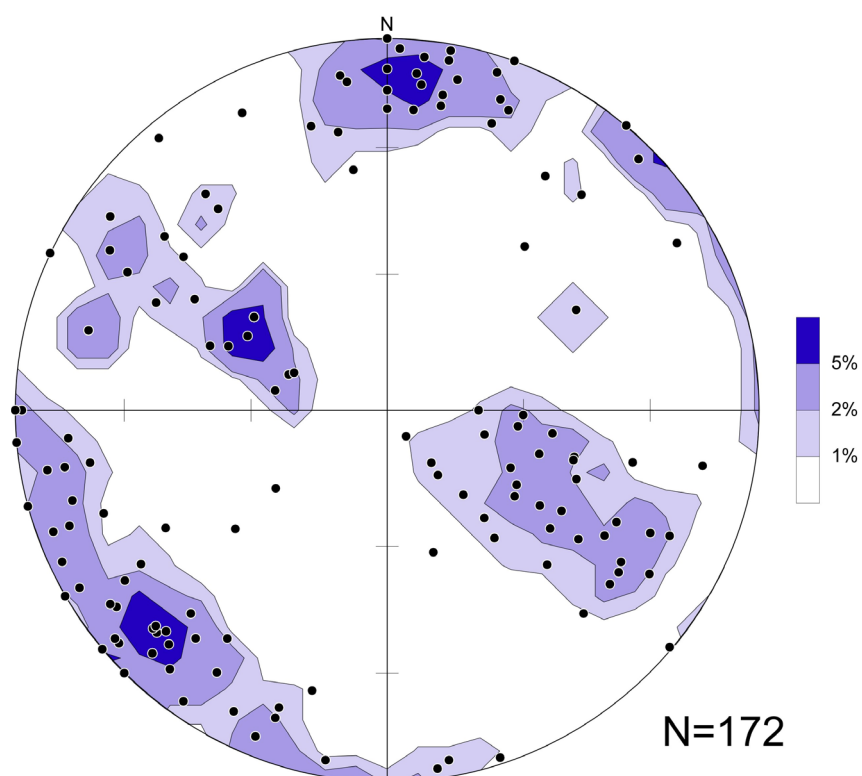


Figure 16. Stereonet of poles to all surface fractures in the South Peak area. Contours at 1%, 2% and 5% of data per 1% of net.

A total of 151 fractures with apertures <1 cm (commonly ≤ 1 mm) were also identified and measured in the image logs of the drillhole. Their orientations are more variable than the open (and likely larger) fractures, but the larger sample size provides more statistically valid results. The three most frequently encountered orientations dip west-northwest (subparallel to bedding), east-southeast and east-northeast (Figure 17). These fracture patterns show good correspondence with fractures measured in outcrop. The two main differences between the plots are the lack of vertical beds measured in the borehole due to the low probability of intersecting surfaces subparallel to the borehole. The fewer azimuths represented in the surface data may be due to human bias — the tendency to look for patterns and sets rather than measuring every orientation in outcrop, as is done with borehole data.

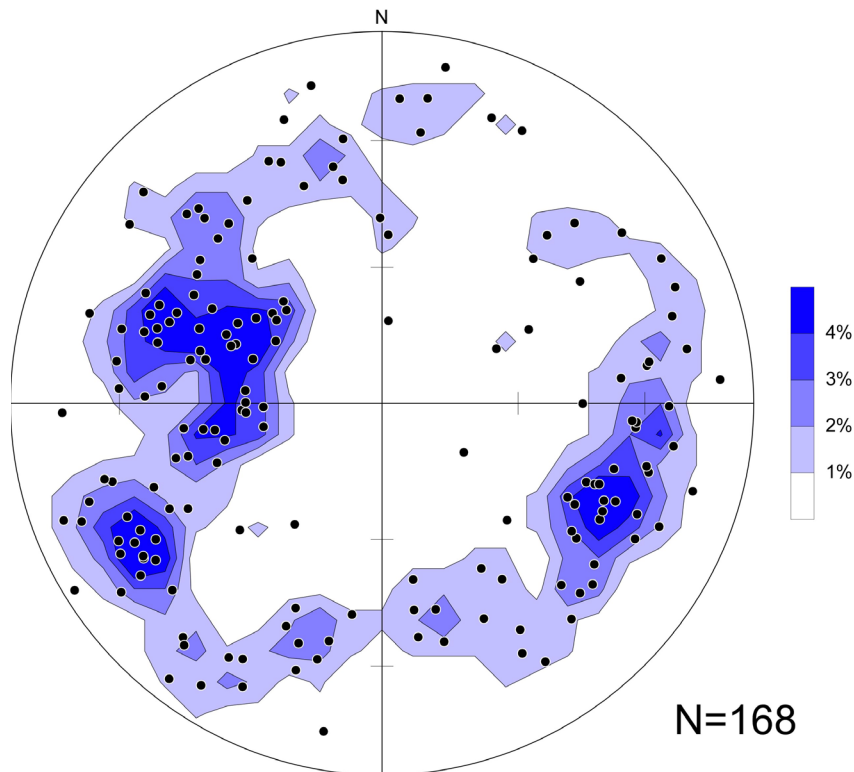


Figure 17. Stereoplot of poles to all fractures and major fractures in the borehole. Contours at 1%, 2%, 3% and 4%.

Mean densities and spacing for all fractures measured along the three scan lines and in the borehole (see Figure 10 for locations) are summarized in the table below. Higher fracture densities were observed in exposed rocks compared to in the borehole. This could be explained several ways: 1) we can see even the healed and hairline fractures at the surface with the naked eye, but they would be more difficult to see in digital optical borehole televiewer images; 2) they are under lower confining pressures and have room to expand during freeze-thaw cycles, so there may actually be more fractures at the surface; 3) the scan lines are close to large fissures and may cross localized fracture swarms. In the borehole images the major open (> 1.0 cm) fractures were distinguished from the rest; they are rarer, but important, because their 2.29 m mean spacing indicates that blocks of this size would be expected in future mass-wasting events. Such sizes are common in the 1903 Frank Slide mass, as are decimetre-scale blocks.

Table 1. Fracture density and spacing in outcrop and borehole.

<u>Mean</u>	Crack #1 scan line	Crack #2 scan line	Scan line near borehole	Borehole
Fracture density	13.50 per metre	9.09 per metre	11.96 per metre	4.24 per metre
Fracture spacing	7.41 cm	11.00 cm	8.36 cm	23.60 cm
Open (>1 cm) fracture density				0.44 per metre
Open (>1 cm) fracture spacing				2.29 m

The drillhole data can be compared to the interpreted surfaces in a Ground Penetrating Radar (GPR) dataset collected by Theune et al. (2006), along their Line B, which trends 057° relative to true north

(for location see Figure 10). The orientations of mean bedding (red) and of all the major fractures (>1 cm) in the borehole were plotted on the interpretation of the GPR data as apparent dips in the plane of the section (Figure 18). The density of discontinuities recognized in the GPR data is of the same order of magnitude as the density of open (>1 cm) fractures in the borehole, supporting the theory that it is the open features that are most likely to be imaged in GPR data. Fractures in the borehole that have apparent dips to the SW are coloured blue and are consistent with the steeper-than-bedding fractures seen at the surface. These orientations are also interpreted in the GPR data. There are several sets of fractures with apparent dips to the NE that are coloured black. Most are not imaged in the GPR data because they are nearly perpendicular to the ground along the chosen line of acquisition. These large fractures have the most dangerous orientations because they dip toward the Frank Slide surface and the town of Bellevue.

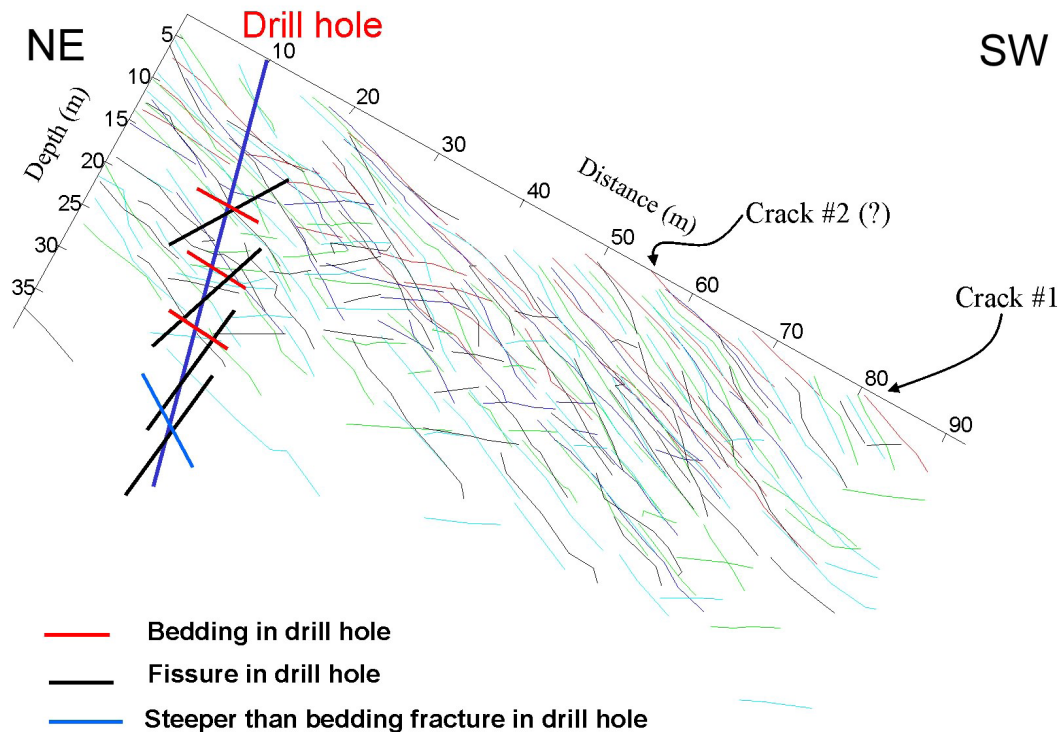


Figure 18. Borehole data (heavy lines) superimposed on GPR data interpretation (thin lines) of Theune et al., 2006. Notice that Cracks #1 and #2 are not imaged on this line. The location of the GPR line is shown in Figure 10.

4 Implications for Slope Stability

The 1903 Frank Slide was originally described as occurring along fracture planes perpendicular to bedding in a west-dipping monocline (McConnell and Brock, 1904). Later interpretation was based on inferred movements along bedding planes on the east limb of the Turtle Mountain anticline (Cruden and Krahn, 1973; Fossey, 1986).

Two potential kinematic models of slope failure can be distinguished: sliding and toppling. Both processes are presently observed on Turtle Mountain. The 1903 slide is the best example of sliding, and a large rock fall that occurred in 2001 is a good example of toppling. Failure of a large rock mass is possible if discontinuities exist in the rock. In the South Peak area, these discontinuities are the bedding planes and the fractures (including fissures). The east-northeast-dipping fissures, which dip to the Frank Slide surface and the town of Bellevue, are the more likely ones to fail and, together with sliding along

bedding planes along the east limb of the Turtle Mountain anticline, this could result in a major rock slide toward Bellevue (Read et al., 2005). Historical (Allan, 1933) and more recent (BGC, 2000; Jaboyedoff et al., in press) suggest that a failure with a volume of up to 5.5 million m³ is kinematically feasible. A more detailed discussion of mechanisms is provided by Moreno and Froese (2006).

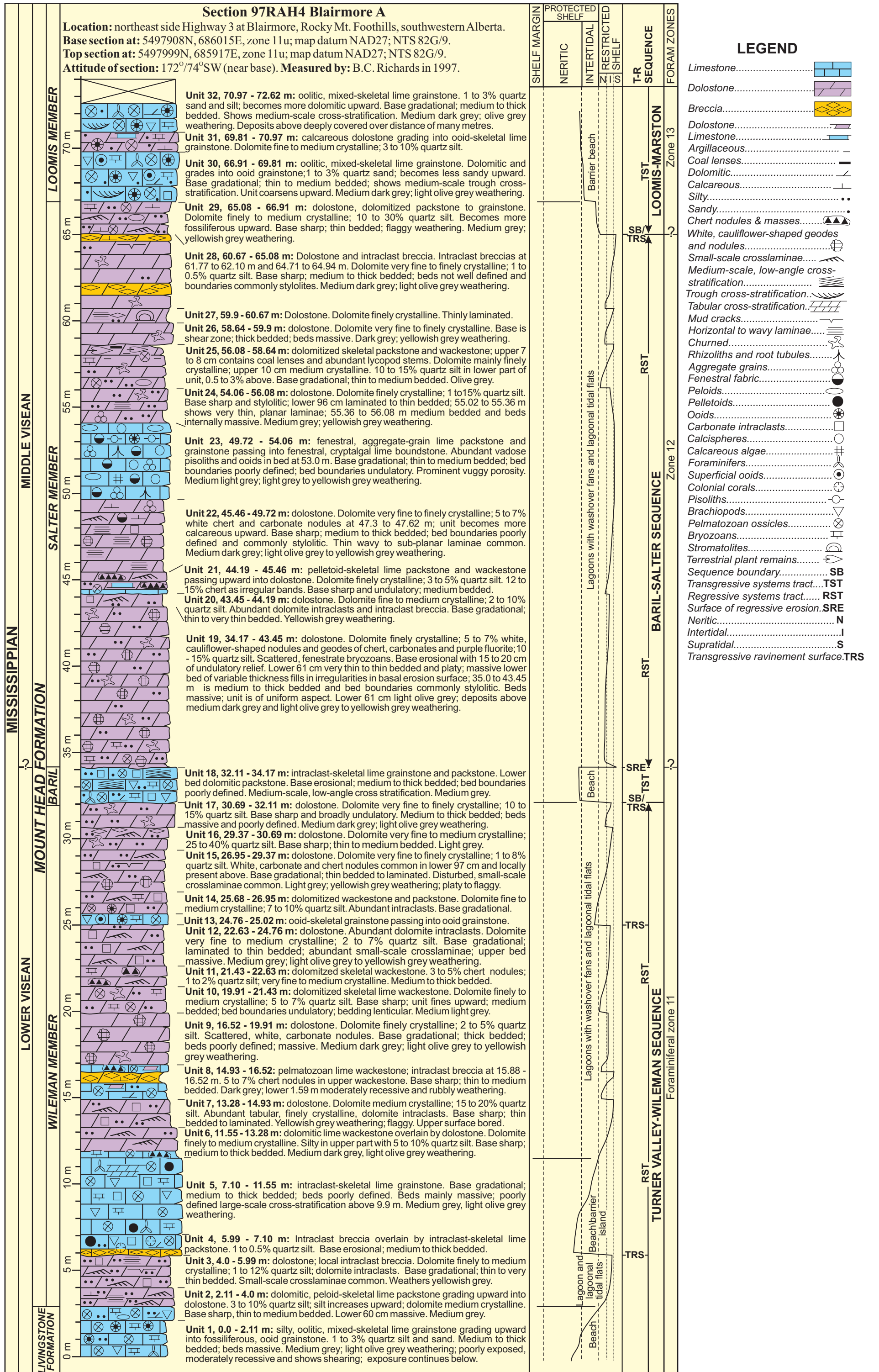
Normal faults are the main structures causing topple failure. They are slightly more likely to occur in the North Peak area and the resulting slides will generally be smaller in volume than the potential South Peak slide (as shown by the large rock fall from North Peak in 2001).

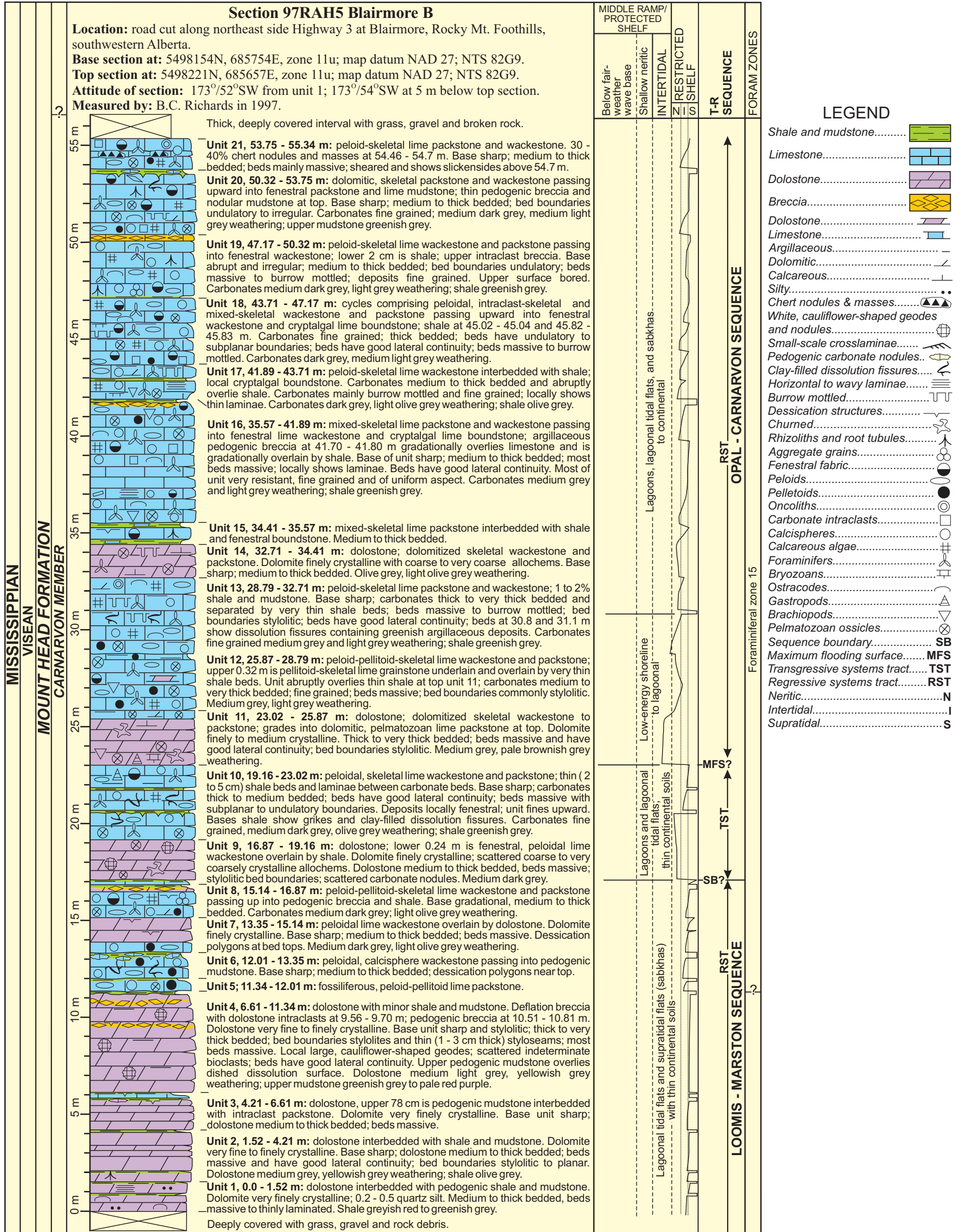
5 References

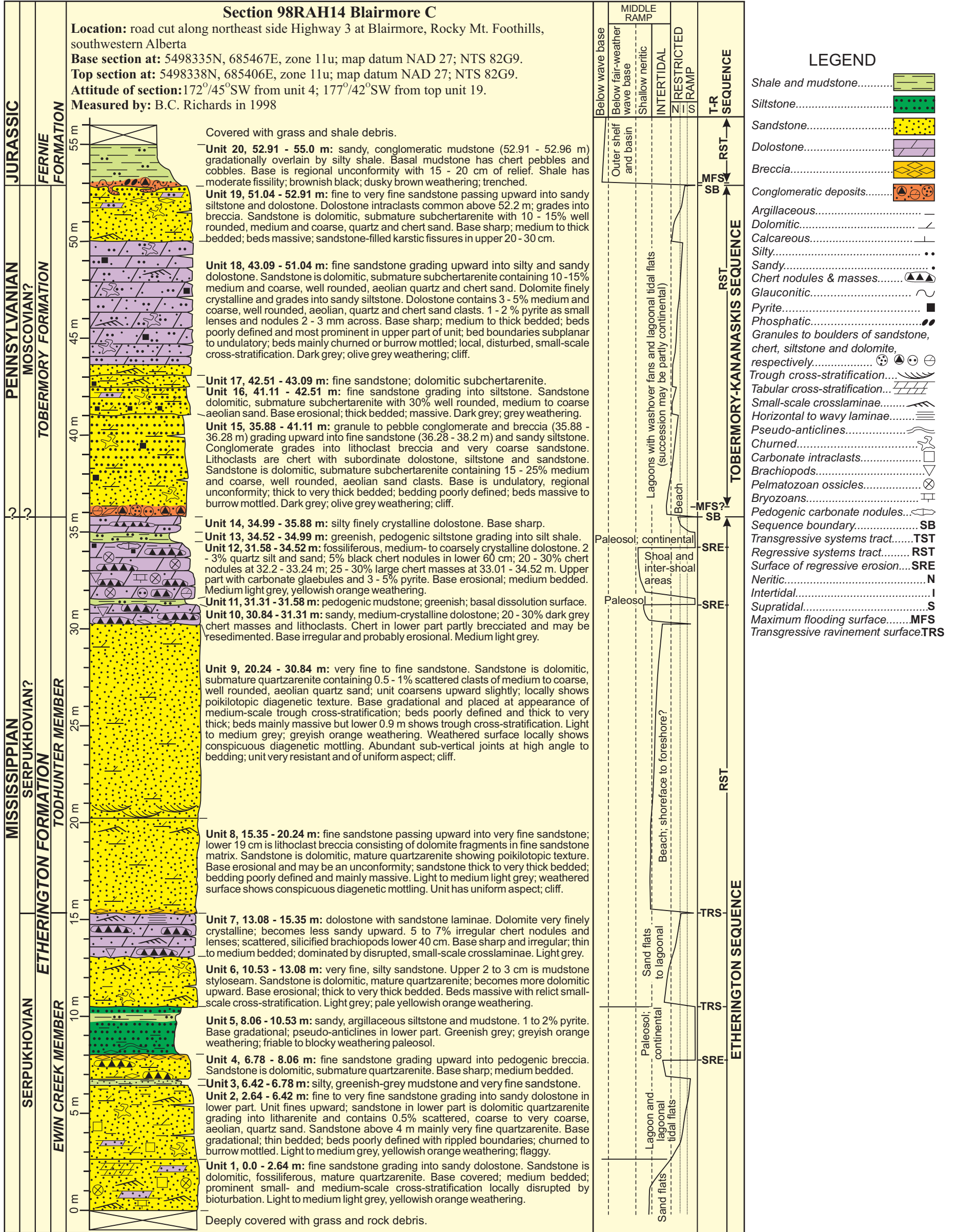
- Allan, J.A. (1931): Report on stability of Turtle Mountain, Crowsnest District, Alberta; Dept. of Public Works, Alberta Provincial Archives, 14 p.
- Allan, J.A. (1932): Second report on stability of Turtle Mountain, Crowsnest District, Alberta; Dept. of Public Works, Alberta Provincial Archives, 25 p.
- Allan, J.A. (1933): Report on stability of Turtle Mountain, Alberta and survey of fissures between North Peak and South Peak; Dept. of Public Works, Alberta Provincial Archives, 28 p.
- BGC Engineering Inc. (2000): Geotechnical hazard assessment of the south flank of Frank Slide, Hillcrest, Alberta; Prepared for Alberta Environment, Contract No. 00-0153, 43 p.
- Bidwell, A., Froese, C.R., Anderson, W.S. and Cavers, D.S. (2005): Geotechnical drilling on the South Peak of Turtle Mountain; 58th Canadian Geotechnical Conference, Saskatoon, 8 p.
- Charlesworth, H.A.K., Langenberg, C.W. and Ramsden, J. (1976): Determining axes, axial planes, and sections of macroscopic folds using computer-based methods; Canadian Journal of Earth Sciences, v. 13, p. 54-65.
- Chen, Z., Stewart, R.R. and Bland, H.C. (2005): Analysis of microseismicity at a mountain site; CREWES Research Report, University of Calgary, v.17, chap. 7, p. 1-28.
- Cruden, D.M. and Krahn, J. (1973): A re-examination of the geology of the Frank Slide; Canadian Geotechnical Journal, v. 10, p. 581-591.
- Fossey, K.W. (1986): Structural geology and slope stability of the southeast slopes of Turtle Mountain, Alberta; M.Sc. thesis, University of Alberta, 113 p.
- Gibson, D.W. (1985): Stratigraphy, sedimentology and depositional environments of the coal-bearing Jurassic-Cretaceous Kootenay Group, Alberta and British Columbia; Geological Survey of Canada, Bulletin 357, 108 p.
- Jaboyedoff, M., Couture, R. and Locat, P. (in press): Structural analysis of Turtle Mountain (Alberta) using digital elevation model: toward a progressive failure by “toppling” of gently dipping wedges; Geomorphology.
- LaPointe, P.R. and Hudson, J.A. (1985): Characterization and interpretation of rock mass joint patterns; Geological Society of America, Special Paper 199, p. 1-25.
- Leckie, D.A. and Cheel, R.J. (1997): Sedimentology and depositional history of Lower Cretaceous coarse-grained clastics, southwest Alberta and southeast British Columbia; Bulletin of Canadian Petroleum Geology, v. 45, p. 1-24.
- Leckie, D.A. and Krystinik, L.F. (1995): Cretaceous igneous-clast conglomerate in the Blairmore Group, Rocky Mountain Foothills and adjacent subsurface (Bow Island Formation), Alberta, Canada; Bulletin of Canadian Petroleum Geology, v. 43, p. 320-342.
- MacKay, B.R. (1933): Geology and coal deposits of Crowsnest Pass area, Alberta; Geological Survey of Canada, Summary Report, 1932, Part B, p. 21-67.
- Moreno, F. and Froese, C. (2006): Turtle Mountain field laboratory monitoring and research summary report, 2005; Alberta Energy and Utilities Board, EUB/AGS Earth Sciences Report 2006-07, 94 p.
- McConnell, R.G. and Brock, R.W. (1904): Report on the great landslide at Frank, Alberta, Department of the Interior, Annual Report for 1903, Ottawa, Part 8, 17 p.

- Norris, D.K. (1993): Geology and structure cross-sections, Blairmore (West Half), Alberta; Geological Survey of Canada, Map 1829A, scale 1:50 000.
- Price, R.A. (1962): Fernie map-area, east-half, Alberta and British Columbia; Geological Survey of Canada, Paper 61-24, 65 p.; includes Geological Survey of Canada, Map 35-1961, scale: 1 inch = 2 miles.
- Read, R.S., Langenberg, W., Cruden, D., Field, M., Stewart, R., Bland, H., Chen, Z., Froese, C.R., Cavers, D.S., Bidwell, A.K., Murray, C., Anderson, W.S., Jones, A., Chen, J., McIntyre, D., Kenway, D., Bingham, D.K., Weir-Jones, I., Seraphim, J., Freeman, J., Spratt, D., Lamb, M., Herd, E., Martin, D., McLellan, P. and Pană, D. (2005): Frank Slide a century later: the Turtle Mountain monitoring project; in *Landslide Risk Management*, O. Hungr, R. Fell, R.R. Couture and E. Eberhardt (ed.), p. 713–723.
- Richards, B.C., Mamet, B.L. and Bamber, E.W. (2000): Carboniferous sequence stratigraphy, biostratigraphy, and basin development in the vicinity of the Bow Corridor, southwestern Alberta; *GeoCanada 2000–The Millennium Geoscience Summit, Field Trip Guidebook*, 190 p.
- Richards, B.C., Barclay, J.E., Bryan, D., Hartling, A., Henderson, C.M. and Hinds, R.C. (1994): Carboniferous strata of the western Canada sedimentary basin; *in Geological Atlas of the Western Canada Sedimentary Basin*, G.D. Mossop and I. Shetson (comp.), Canadian Society of Petroleum Geologists and Alberta Research Council, Special Report 4, p. 221-250.
- Scott, D.L. (1964): Pennsylvanian stratigraphy; *Bulletin of Canadian Petroleum Geology*, v. 12, Flathead Valley Guidebook Issue, p. 460-493.
- Spratt, D.A. and Lamb, M.A. (2005): Borehole data interpretation and orientations, Turtle Mountain Monitoring Project; *Internal Report of Work Package WP15B*, Alberta Municipal Affairs, 15 p.
- Theune, U., Rokosh, D., Sacchi, M.D. and Schmitt, D.R. (2006): Mapping fractures with GPR: a case study from Turtle Mountain, *Geophysics*, v. 71, B139-B150.
- van der Pluijm, B.A., Vrolijk, P.J., Pevear, D.R., Hall, C.M., and Solum, J.G. (2006): Fault dating in the Canadian Rocky Mountains: evidence for late Cretaceous and early Eocene orogenic pulses; *Geology*, v. 34, p. 837-840.
- Vermilye, J.M., and Scholz, C.H. (1995): Relation between vein length and aperture; *Journal of Structural Geology*, v. 17, p. 423-434.

Appendix 1. Section 97RAH4 Blairmore A







Appendix 4. Open Fissures near South Peak

		UTM NAD83 zone 11						
	Station ID	Easting	Northing	Dip direction	Dip	Width (m)	Depth (m)	Comment
Crack #1-1 east	141	687043	5494916	115	90	0.15		
Crack #1-1 west.	141	687043	5494916	90	90	0.15		
Crack #1-2A	142	687042	5494936	75	90	0.10		
Crack #1-2A	142	687042	5494936	222	67	0.10		
Crack #1-2B	183-1	687040	5494940	80	70	0.20		
Crack #1-2C	183	687037	5494949	185	70	0.29		
Crack #1-3	142-1	687042	5494939	85	90	0.20		
Crack #1-3	142-1	687042	5494939	50	90	0.20		
Crack #1-4	144	687048	5494972	70	80	0.28		
Crack #1-A		687058	5494943	20	77	0.23		
Crack #1-B	143	687051	5494948	45	73	0.28		
Crack #1-C		687049	5494952	190	85	0.20	7	
Crack #1-D		687047	5494954	70	85	0.44		
Crack #1-E		687044	5494956	200	78	0.40		
Crack #1-F		687039	5494958	190	75	0.77		
Crack #1-G		687035	5494960	202	76	0.44		
Crack #1-H		687032	5494962	45	90	0.39		
Crack #1-I		687029	5494963	190	72	0.62		
Crack #1-J		687021	5494974	65	86	0.20		
Crack #2-1	145-1	687054	5494990	70	70	0.70		
Crack #2-2	145-2	687052	5494993	80	77	0.70		
Crack #2-A	145	687054	5494988	57	73	0.70		
Crack #2-B		687051	5494990	74	77	0.90		
Crack #2-C		687047	5494994	35	85	1.00		
Crack #2-D		687040	5494999	50	85	1.10		
Crack #2E	165	686999	5495054	55	80	1.50	10	
Crack #3	163	687100	5495027	60	85	0.37		
Crack #3	163	687100	5495027	70	85	0.37		
Crack #3	163	687100	5495027	140	85	0.37		
Crack(@seism. stn)	187	687380	5494779	217	85	0.10		not on ridge

Appendix 5. Fractures Measured in Scan Line near Borehole

Orientation:	N252; Plunge 16	
location	E0687045	N5495043
cm from N end	Dip direction	Dip
2	225	85
4	105	72
5.5	105	72
8.5	225	85
17	105	72
20	105	72
24	225	85
30	105	72
44	220	48
51	200	90
53	225	85
56	225	85
62	85	75
66	10	85
82	52	43
92	35	64
120	198	85
128	214	65
140	180	90
150	180	70
156	33	73
160	33	73
170	15	67
173	22	84
182	240	79
198	22	84
204	220	90
220	170	65
225	170	65
233	200	71
238	125	80
250	125	80
255	40	69
258	40	69
274	120	50

Orientation:	N252; Plunge 16	
location	E0687045	N5495043
cm from N end	Dip direction	Dip
284	120	50
288	40	80
297	60	90
300	120	75
344	190	88
361	43	75
379	49	85
393	44	80
397	44	80
405	185	80
474	47	75
377	27	80
481	47	74
484	47	74
486	47	74
487	118	68
489	118	68
494	44	65
496	44	65
498	44	65
503	125	36
505	125	36
506	125	36
507	125	36
508	125	36
509	125	36
510	125	36
515	125	36
531	127	58
533	54	79
534	118	35
552	115	58
563	58	67
577	173	78

Appendix 6. Fractures Measured in Scan Line Near Crack #1

Orientation: N190; Plunge 30		
location:	E687048	N5494958
cm from N end	Dip direction	Dip
0	318	32
8	110	42
19	112	38
70	284	43
72	278	37
76	306	45
85	295	30
92	286	35
103	342	33
107	296	58
122	270	20
124	277	29
130	294	72
137	186	77
145	280	75
153	308	65
155	310	89
182	182	87
185	180	81
192	342	88
196	20	74
200	242	48
204	242	48
212	186	85
218	154	78
226	290	45
229	172	80
230	172	80
232	172	80
237	282	57
240	285	43
247	295	67
250	295	67
254	180	75
255	180	75
257	180	75
277	165	68
285	80	82
287	80	82
297	185	70
311	90	88
317	90	88

Appendix 7. Fractures Measured in Scan Line near Crack #2

Orientation:	N170; Plunge 35		
location	E687054	N5494988	
cm from N end	Dip direction	Dip	
0	352	87	
6	316	65	
9	324	7	
14	305	65	
18	303	64	
31	302	72	
36	350	85	
47	300	33	
72	304	52	bedding
74	314	50	bedding
79	320	37	
85	318	25	
100	322	18	
112	272	30	
113	320	15	
117	284	22	
119	304	34	
152	55	30	
160	140	65	
161	110	23	
179	192	80	
180	110	23	
216	140	60	
220	112	22	
234	128	65	
257	46	75	
290	300	45	
298	302	40	
303	300	57	bedding
313	62	57	
350	100	25	
352	172	55	

Appendix 8. All Subsurface Structural Data (from Borehole)

Depth (m)	Dip Azimuth (Mag North)	Dip Azimuth (True North)	Dip	Class	Notes
19.09			0	bottom casing	casing affected magnetometer → unoriented image
20.84			0	tool zeroed	
21.27	276.5	293.2	38.8	bedding	disseminated circular vugs ~1cm diameter
21.32	270.4	287.1	40.9	bedding	
21.42	143.5	160.2	52.1	fracture	
21.50	95.3	112.0	34.9	fracture	
21.51	281.4	298.1	56.0	fracture	
21.53	277.3	294.0	38.8	bedding	5x10mm vugs
21.55	245.2	261.9	61.2	fracture	
21.57	298.7	315.4	58.1	fracture	
21.60	271.2	287.9	34.0	bedding	5x10mm vugs
21.80	285.8	302.5	30.6	bedding	
21.85	89.2	105.9	62.0	fracture	
21.87	286.6	303.3	32.7	bedding	5x10mm vugs
21.95	286.2	302.9	32.4	bedding	
21.99	286.6	303.3	33.6	bedding	
22.00	289.7	306.4	32.4	bedding	
22.04	277.3	294.0	35.1	bedding	
22.07	95.5	112.2	44.1	fracture	
22.10	284.3	301.0	34.2	bedding	
22.17	276.1	292.8	34.5	bedding	
22.25	285.0	301.7	33.6	bedding	
22.32	273.2	289.9	29.4	bedding	
22.40	282.6	299.3	30.6	bedding	
22.45	108.1	124.8	50.8	fracture	
22.50	277.0	293.7	54.9	fracture	
22.53	108.6	125.3	72.1	fracture	
22.54	253.4	270.1	44.9	fracture	
22.57	285.5	302.2	31.0	bedding	
22.61	282.0	298.7	32.7	bedding	
22.70	268.8	285.5	32.7	bedding	
22.73	288.1	304.8	53.5	fracture	
22.75	280.2	296.9	46.6	fracture	
22.86	111.5	128.2	52.3	fracture	
22.92	118.4	135.1	52.5	fracture	
22.95	258.8	275.5	58.0	fracture	
22.97	257.6	274.3	58.1	fracture	

Depth (m)	Dip Azimuth (Mag North)	Dip Azimuth (True North)	Dip	Class	Notes
23.00	257.3	274.0	57.0	fracture	
23.00	265.9	282.6	36.0	bedding	
23.08	267.8	284.5	63.2	fracture	
23.12	58.0	74.7	45.0	fracture	
23.12	269.1	285.8	54.6	fracture	
23.16	274.4	291.1	49.2	fracture	
23.17	103.2	119.9	48.8	fracture	
23.20	287.3	304.0	51.6	fracture	
23.26	281.0	297.7	48.9	fracture	
23.20	74.9	91.6	53.7	fracture	
23.30	274.1	290.8	51.3	fracture	
23.36	280.1	296.8	36.8	bedding	
Depth (m)	Dip Azimuth (Mag North)	Dip Azimuth (True North)	Dip	Class	Notes
23.37	97.1	113.8	50.5	fracture	
23.41	280.3	297.0	34.0	bedding	
23.46	94.2	110.9	56.4	fracture	
23.59	309.0	325.7	47.8	fracture	
23.63	23.7	40.4	71.5	fracture	
23.63	312.3	329.0	43.0	fracture	
23.69	328.7	345.4	55.9	fracture	
23.83	334.5	351.2	46.9	fracture	
24.02	281.5	298.2	66.2	fracture	
24.27	88.4	105.1	52.5	major fracture	
24.36	71.6	88.3	75.0	fracture	
24.61	283.5	300.2	40.5	bedding	
24.76	274.0	290.7	41.6	bedding	
24.93	274.0	290.7	43.9	bedding	
25.18	273.2	289.9	42.3	bedding	
25.21	272.4	289.1	42.0	bedding	
25.33	275.3	292.0	42.3	bedding	
25.80	129.7	146.4	55.2	fracture	
25.98	278.9	295.6	27.6	bedding	
26.03	290.2	306.9	30.3	bedding	
26.17	273.0	289.7	44.9	bedding	
26.26	273.2	289.9	49.6	bedding	
26.36	262.4	279.1	48.6	bedding	
26.64	165.4	182.1	37.4	fracture	
26.71	207.8	224.5	53.2	fracture	

Depth (m)	Dip Azimuth (Mag North)	Dip Azimuth (True North)	Dip	Class	Notes
26.84	140.5	157.2	59.6	fracture	
26.88	311.9	328.6	60.6	fracture	
27.01	291.6	308.3	45.0	bedding	
27.10	296.3	313.0	38.0	bedding	
27.15	299.7	316.4	43.0	bedding	
27.19	107.3	124.0	33.6	fracture	
27.23	91.7	108.4	53.6	fracture	
27.36	114.8	131.5	74.6	fracture	
27.55	285.4	302.1	32.0	bedding	
27.61	288.3	305.0	37.0	bedding	
27.71	270.2	286.9	42.0	bedding	
27.83	78.6	95.3	30.3	fracture	
27.87	71.5	88.2	26.1	fracture	
27.88	274.2	290.9	37.2	bedding	
27.90	70.5	87.2	31.0	fracture	
27.96	281.7	298.4	33.1	bedding	
27.96	287.1	303.8	34.7	bedding	
28.02	286.5	303.2	33.3	bedding	
28.09	294.0	310.7	63.8	fracture	
28.17	278.9	295.6	39.2	bedding	
28.29	263.7	280.4	32.9	bedding	
28.90	86.0	102.7	43.9	fracture	
29.03	280.1	296.8	39.2	bedding	
29.05	333.3	350.0	39.8	fracture	
Depth (m)	Dip Azimuth (Mag North)	Dip Azimuth (True North)	Dip	Class	Notes
29.11	328.7	345.4	47.8	fracture	
31.06	43.9	60.6	65.4	fracture	
32.30	291.7	308.4	48.4	bedding	
32.58	299.2	315.9	38.8	bedding	
32.66	297.6	314.3	42.2	bedding	
32.90	117.5	134.2	29.4	fracture	
32.96	112.7	129.4	31.3	fracture	
32.99	119.2	135.9	31.3	fracture	
33.17	295.4	312.1	33.1	bedding	
33.27	307.0	323.7	34.7	bedding	
33.36	387.1	43.8	38.0	bedding	
33.49	270.3	287.0	38.4	bedding	
33.62	138.2	154.9	61.1	fracture	

Depth (m)	Dip Azimuth (Mag North)	Dip Azimuth (True North)	Dip	Class	Notes
33.87	120.0	136.7	61.2	fracture	
33.98	119.5	136.2	58.4	fracture	
34.15	271.1	287.8	41.8	bedding	
34.25	263.1	279.8	39.3	bedding	
34.35	263.5	280.2	35.8	bedding	
34.42	184.3	201.0	71.1	fracture	
34.43	276.1	292.8	57.6	fracture	
34.61	166.6	183.3	70.9	fracture	
34.61	300.4	317.1	33.6	bedding	
34.80	150.7	167.4	76.5	fracture	
35.54	153.3	170.0	51.1	fracture	
35.76	98.3	115.0	59.5	fracture	
36.05	97.1	113.8	55.2	fracture	
36.20	62.1	78.8	26.6	fracture	
36.20	264.9	281.6	41.8	bedding	
36.25	275.2	291.9	39.6	bedding	
36.31	227.8	244.5	27.9	fracture	
36.37	278.0	294.7	37.4	bedding	
36.71	121.4	138.1	43.4	fracture	
37.59	40.3	57.0	65.5	fracture	
37.79	51.8	68.5	75.8	major fracture	
38.28	89.3	106.0	42.2	fracture	
38.30	87.2	103.9	40.5	fracture	
38.38	292.7	309.4	32.8	bedding	
38.47	53.1	69.8	55.1	fracture	
38.78	277.3	294.0	37.4	bedding	
39.04	40.7	57.4	65.3	fracture	
39.14	171.8	188.5	71.8	fracture	
39.20	37.4	54.1	75.6	fracture	
39.27	54.7	71.4	72.0	fracture	
39.51	22.6	39.3	73.0	fracture	
39.61	334.5	351.2	53.5	fracture	
39.67	45.7	62.4	68.9	fracture	
39.69	269.1	285.8	75.8	fracture	
39.78	256.7	273.4	46.9	bedding	
39.86	53.5	70.2	39.0	fracture	
Depth (m)	Dip Azimuth (Mag North)	Dip Azimuth (True North)	Dip	Class	Notes
39.98	351.4	8.1	47.9	fracture	

Depth (m)	Dip Azimuth (Mag North)	Dip Azimuth (True North)	Dip	Class	Notes
40.07	6.6	23.3	55.0	fracture	
40.15	76.5	93.2	60.2	fracture	
40.20	37.8	54.5	68.7	major fracture	
40.21	302.0	318.7	66.2	fracture	
40.34	297.1	313.8	62.9	fracture	
40.56	14.4	31.1	68.8	major fracture	
41.10	44.8	61.5	49.7	fracture	
41.64	270.6	287.3	42.3	bedding	
41.79	274.9	291.6	39.4	bedding	
41.79	273.7	290.4	52.3	fracture	
41.83	82.3	99.0	61.5	fracture	
42.09	31.6	48.3	42.5	fracture	
42.30	2.5	19.2	57.8	fracture	
42.41	53.1	69.8	80.4	major fracture	
42.58	45.6	62.3	62.6	major fracture	
42.95	278.6	295.3	45.4	bedding	
43.44	273.3	290.0	39.0	bedding	
43.50	272.4	289.1	39.4	bedding	
43.56	257.2	273.9	43.7	bedding	
43.59	244.5	261.2	61.9	fracture	
43.63	267.5	284.2	40.5	bedding	
43.70	221.7	238.4	52.5	fracture	
43.74	314.0	330.7	66.1	fracture	
43.78	43.4	60.1	70.1	fracture	
43.80	217.9	234.6	68.1	fracture	
43.83	49.3	66.0	64.1	fracture	
43.95	65.0	81.7	40.2	fracture	
44.10	144.2	160.9	69.6	fracture	
44.21	6.2	22.9	50.0	fracture	
44.36	262.3	279.0	40.3	bedding	
44.56	122.8	139.5	53.4	fracture	
44.63	90.4	107.1	71.2	fracture	
44.69	9.5	26.2	73.9	major fracture	
44.89	57.1	73.8	64.6	fracture	
45.26	31.6	48.3	64.6	fracture	
45.27	236.6	253.3	70.4	fracture	
45.43	66.1	82.8	44.7	fracture	
45.48	225.9	242.6	73.5	fracture	
45.57	42.0	58.7	86.4	major fracture	

Depth (m)	Dip Azimuth (Mag North)	Dip Azimuth (True North)	Dip	Class	Notes
45.57	253.9	270.6	66.2	fracture	
45.68	277.3	294.0	70.5	fracture	
45.73	102.4	119.1	43.4	fracture	
46.45	190.5	207.2	71.3	fracture	
46.59	42.3	59.0	60.3	major fracture	
46.77	318.0	334.7	53.9	fracture	
46.89	210.2	226.9	60.2	fracture	
47.07	151.6	168.3	54.7	fracture	
48.21	60.1	76.8	35.8	fracture	
Depth (m)	Dip Azimuth (Mag North)	Dip Azimuth (True North)	Dip	Class	Notes
48.29	90.0	106.7	56.4	major fracture	
49.25	284.2	300.9	39.0	bedding	
49.32	287.6	304.3	37.8	bedding	
49.46	294.0	310.7	33.8	bedding	
49.65	302.4	319.1	33.1	bedding	
49.78	300.5	317.2	34.7	bedding	
49.95	288.2	304.9	36.6	bedding	
50.07	295.4	312.1	33.1	bedding	
50.18	295.0	311.7	35.5	bedding	
50.22	300.4	317.1	32.4	bedding	
50.42	279.2	295.9	38.8	bedding	
50.58	264.3	281.0	41.1	bedding	
50.70	259.6	276.3	42.5	bedding	
50.89	257.9	274.6	37.8	bedding	
51.03	281.9	298.6	43.4	bedding	
51.15	277.7	294.4	38.4	bedding	
51.26	284.7	301.4	39.4	bedding	
51.36	38.6	55.3	63.2	fracture	
51.49	16.0	32.7	79.2	fracture	
51.57	290.5	307.2	60.9	fracture	
51.62	94.2	110.9	51.3	fracture	
51.75	279.4	296.1	55.7	fracture	
51.88	58.4	75.1	47.9	fracture	
52.02	174.0	190.7	81.1	fracture	
52.10	58.0	74.7	66.4	fracture	
52.47	296.4	313.1	38.0	fracture	
52.51	243.2	259.9	72.2	fracture	
52.52	19.1	35.8	33.0	fracture	

Depth (m)	Dip Azimuth (Mag North)	Dip Azimuth (True North)	Dip	Class	Notes
52.56	46.9	63.6	53.7	fracture	
52.56	226.6	243.3	36.4	fracture	
52.77	21.0	37.7	83.0	major fracture	
53.21	247.3	264.0	54.4	fracture	
53.58	154.9	171.6	61.1	fracture	
54.84	261.7	278.4	68.2	fracture	
55.98	171.4	188.1	62.7	fracture	
56.03	241.8	258.5	44.7	bedding	
56.24	281.0	297.7	44.7	bedding	
56.31	275.8	292.5	44.5	bedding	
56.41	270.8	287.5	38.0	bedding	
56.47	260.8	277.5	38.4	bedding	
56.62	266.7	283.4	62.3	major fracture	
57.78	73.6	90.3	30.1	fracture	
58.04	281.2	297.9	44.7	bedding	
58.21	77.7	94.4	49.7	fracture	
58.34	103.6	120.3	27.1	fracture	
58.44	97.1	113.8	37.8	fracture	
58.53	92.2	108.9	30.1	fracture	
58.55	94.1	110.8	35.8	fracture	
58.58	102.3	119.0	36.6	fracture	
Depth (m)	Dip Azimuth (Mag North)	Dip Azimuth (True North)	Dip	Class	Notes
58.61	167.7	184.4	18.1	fracture	
58.63	265.1	281.8	34.0	bedding	
58.70	64.2	80.9	37.6	fracture	
58.70	271.2	287.9	34.9	bedding	
58.81	265.9	282.6	32.7	bedding	
59.02	231.7	248.4	73.7	fracture	
59.41	69.4	86.1	30.1	fracture	
59.55	117.4	134.1	62.3	fracture	
59.61	1.2	17.9	64.5	major fracture	
59.63	355.9	12.6	55.2	fracture	
59.78	162.7	179.4	41.3	major fracture	
60.12	276.8	293.5	63.9	fracture	
60.27	311.0	327.7	71.1	fracture	
60.32	284.3	301.0	20.9	fracture	
60.36	111.5	128.2	29.6	fracture	
60.40	357.5	14.2	60.3	fracture	

Depth (m)	Dip Azimuth (Mag North)	Dip Azimuth (True North)	Dip	Class	Notes
60.54	353.4	10.1	78.7	major fracture	
60.57	209.6	226.3	46.9	fracture	
60.84	249.3	266.0	80.3	fracture	
60.92	253.4	270.1	42.3	bedding	
60.95	11.9	28.6	67.3	major fracture	